PROCEEDINGS OF SCIENCE

An introduction to BKL theory

Marine De Clerck[a,*]

[a] *University of Cambridge,*
Wilberforce Rd, Cambridge CB3 0WA, United Kingdom

E-mail: md989@cam.ac.uk

These notes summarize six hours of lectures given at the 20th edition of the Modave Summer School in Mathematical Physics on the topic of the Belinskii, Khalatnikov and Lifshitz (BKL) theory. Their work gives a description of the generic oscillatory behavior of solutions to Einstein's equations in the vicinity of a spacelike singularity. In these notes, we introduce the generalized Kasner solution and subsequently study the mixmaster or diagonal Bianchi IX geometry as a toy model for the general near-singularity oscillatory behavior. We give an overview of the cosmological billiard approach and apply it to the mixmaster universe. We briefly discuss the cosmological billiard description of the near-singularity description of inhomogeneous vacuum gravity in four spacetime dimensions. Finally, we derive the Wheeler-DeWitt equation obtained by canonically quantizing the cosmological billiard and give an overview of the peculiar symmetries that appear in this problem. It is an interesting open problem whether these symmetries point to any fundamental feature of (quantum) gravity.

Modave Summer School in Mathematical Physics (Modave2024)
1 September 2024
Modave, Belgium

*Speaker

 ISSN 1824-8039 . Published by SISSA Medialab.

PoS(Modave2024)002

Contents

1 Introduction **2**

2 Einstein's equations in the BKL limit **3**
2.1 The generalized Kasner universe 4
2.2 A toy model for oscillations: the mixmaster universe 8

3 Hamiltonian formalism and the billiard picture **14**
3.1 The cosmological billiard of the mixmaster universe 15
3.2 The Wheeler-DeWitt equation for cosmological billiards 19
3.3 The cosmological billiard of four-dimensional vacuum gravity 20
3.4 Some effects of matter 25
3.5 Cosmological billiards in higher dimensions 27

4 Quantum chaos in cosmological billiards **28**
4.1 Classical chaos in cosmological billiards 28
4.2 Quantum chaos from spectral statistics 30
4.3 Arithmetic quantum chaos 31
4.4 String theories, M-theory and their relation to octonions 34

5 Discussion **35**

1. Introduction

The work by Belinskii, Khalatnikov and Lifshitz (BKL) on near-singularity dynamics [1–6] was sparked by a question formulated by Landau at the end of the fifties. Geometries with singular points known at the time usually came with a large degree of symmetry. It was natural to question then whether the singular behavior in these theories resulted from the symmetric setup or if one could, in fact, find a set of solutions of nonvanishing measure in the space of solutions featuring a singularity. These interrogations were contemporary to Penrose's singularity theorems on geodesic incompleteness [7], which appeared to imply that incomplete geodesics are a generic feature of general relativity. The results of BKL complemented Penrose's work, providing a framework to describe generic local dynamics with a singularity. It is quite remarkable that their efforts culminated in one of the few instances where an analytic description of a generic solution to Einstein's equations could be achieved.

The hypothesis that was instrumental in these developments is the idea that nearby spatial points decouple in the vicinity of a spacelike singularity. The intuitive picture for this decoupling is illustrated in Figure 1. Consider the future lightcone emanating from two neighboring points on

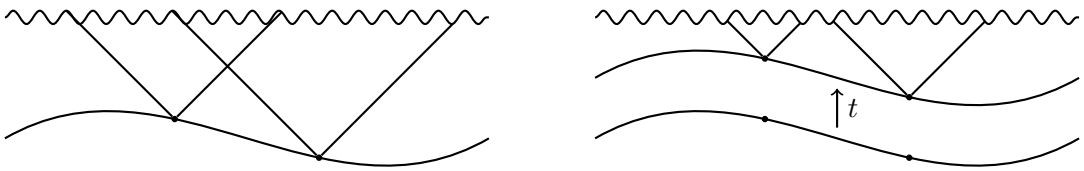

Figure 1: An illustration of the decoupling of spatially separated points. For any initial separation of two points on a spatial slice, there comes a time where the future cones of the two points do not overlap any more.

a spacelike slice. No matter how close the two points, there is always a time in the future where their lightcones reach the singularity before intersecting. This decoupling limit, also known as the ultralocal limit, provided a fruitful approximation in the description of the near-singularity physics and was used by BKL to dramatically simplify Einstein's equations.

The structure of the notes is as follows. At first, we follow the historical development, starting in section 2 by an analysis of Einstein's equations in four spacetime dimensions in the decoupling limit provided by the near-singularity regime. We will discuss the generalized Kasner solution and understand that it does not depict the generic situation. Instead of spending a great deal of time deriving a complete solution, we shall illustrate the generic oscillatory behavior by studying the mixmaster solution. In section 3, we will develop the cosmological billiard description that emerges from a Hamiltonian perspective on the dynamics. The Hamiltonian formalism naturally paves the way to canonical quantization, enabling the study of semiclassical properties of gravity. Due to the decoupling limit, the Wheeler-DeWitt equation is tractable, and the quantum theory is found to have unusual chaotic characteristics, which we review in section 4.

These notes are meant to be a first introduction to the seminal works on near-singularity dynamics, aimed at PhD students. The goal is to provide an overview of the different approaches to describe the classical dynamics close to a singularity, focusing on the main ideas and concepts that form the core of the BKL theory. The three sections of these notes should be viewed as starting points, providing a suitable background for a more in-depth exploration of the literature. At times, we shall dedicate small subsections to side remarks that hopefully give the reader a broader perspective and illustrate that this long-established topic may have more to teach us. For interested and avid readers, we highly recommend the book [8] and the reviews [9, 10] which cover the three main topics of these notes in tremendous detail.

2. Einstein's equations in the BKL limit

In this first section, we work towards an understanding of the generic near-singularity oscillatory behavior of metric components in four dimensional vacuum gravity. We begin with a derivation of the generalized Kasner solution that follows from the ultralocal regime imposed by the singularity in section 2.1. In section 2.2, we illustrate how the curvature of space generically terminates a

Kasner evolution and leads to never-ending oscillatory behavior using the mixmaster universe as a toy model. The addition of matter and generalizations to higher dimensions are discussed in section 3.

Throughout these notes, we employ coordinates adapted to the singularity. A spacelike singularity is understood as the end point of a sequence of non-intersecting spacelike surfaces of decreasing volume where curvature invariants blow up. We shall consider a foliation of spacetime where the singularity happens simultaneously on the entire spatial slice at $t \to 0^+$. The time direction is chosen orthogonal to the spacelike slices (i.e. the shift vector $\vec{N}$ is set to zero). For now, we set the lapse to $n = 1$ and consider the proper time as a preferred coordinate variable. We shall reintroduce the lapse when we move on to the Hamiltonian formulation in the next section. To summarize, we consider the metric

$$\mathrm{d}s^2 = -\mathrm{d}t^2 + g_{ij}(\vec{x}, t)\mathrm{d}x^i\mathrm{d}x^j. \tag{2.1}$$

The coordinates defining such a synchronous reference system are also referred to as Gaussian coordinates and can always be considered locally. The metric (2.1) is not fully gauge-fixed, as we are free to characterize the three-dimensional spatial slices in terms of a different set of spatial coordinates $\vec{x} \to \vec{x}'$ without changing the general form of (2.1). This freedom contains three functions of the spatial coordinates. The fact that the singularity is chosen to happen at $t = 0$ everywhere removes any possible (spatial dependent) gauge-ambiguity in the time variable.

2.1 The generalized Kasner universe

We are interested in the dynamics of the spatial metric $g_{ij}(\vec{x}, t)$ close to the singularity. In terms of (2.1), Einstein's equations in vacuum reduce to

$$R^0_0 = \frac{1}{2}\dot{\kappa} + \frac{1}{4}\kappa^j_i\kappa^i_j = 0 \tag{2.2}$$

$$R^0_i = \frac{1}{2}\left(\nabla_i\kappa - \nabla_j\kappa^j_i\right) = 0 \tag{2.3}$$

$$R^i_j = \frac{1}{2\sqrt{g}}\frac{\mathrm{d}}{\mathrm{d}t}\left(\sqrt{g}\kappa^j_i\right) + {}^{(3)}R^i_j = 0 \tag{2.4}$$

with ${}^{(3)}R_{ij}$ the three-dimensional Ricci tensor, $\kappa_{ij} = \dot{g}_{ij}$ the three-dimensional extrinsic curvature tensor, $\kappa \equiv \kappa_{ij}g^{ij}$ and g the determinant of the spatial metric g_{ij}. We use overhead dots to denote derivatives with respect to t.

The equations (2.2)-(2.3) impose the usual four constraints on initial data and (2.4) are dynamical equations. In order to get familiar with the Kasner geometry, it is instructive to first simplify the problem and solve (2.2)-(2.4) assuming the metric has no spatial dependence $g_{ij}(\vec{x}, t) = g_{ij}(t)$. The contribution of the spatial Ricci tensor to (2.4) vanishes, and the trace of the evolution equations yields

$$\frac{\mathrm{d}}{\mathrm{d}t}\left(\sqrt{g}\kappa^i_i\right) = \frac{\mathrm{d}}{\mathrm{d}t}\left(\sqrt{g}\dot{g}_{ij}g^{ij}\right) = 0. \tag{2.5}$$

In this expression, one recognizes the time derivative of the square root of the metric determinant. We obtain a simple evolution equation for the volume of the spacelike metric, which is straightforwardly solved:

$$\frac{\mathrm{d}^2\sqrt{g}}{\mathrm{d}t^2} = 0 \qquad \Rightarrow \qquad \sqrt{g} = \Lambda t + C. \tag{2.6}$$

The requirement that the singularity be reached at $t = 0$ sets $C = 0$. We therefore find that the volume of the spatial slices decreases toward zero as a linear function of the proper time.[1] We may now solve

$$\frac{\mathrm{d}}{\mathrm{d}t}\left(\sqrt{g}\dot{g}_{ik}g^{kj}\right) = 0 \tag{2.7}$$

for $g_{ij}(t)$. At any instant of time, one can diagonalize the metric and its first derivatives by moving to a different frame

$$g_{ij}(t) = l^{\alpha}{}_{i}\eta_{\alpha\beta}(t)l^{\beta}{}_{j}, \tag{2.8}$$

with $l^{\alpha}{}_{i}$ a time-independent matrix. A concrete approach to find this frame is to first rotate to a basis that diagonalizes the matrix g_{ij} at some instant t. We then rescale the basis vectors so that the diagonal elements are all normalized to 1. Then, we express $\dot{g}_{ij}$ in terms of that basis and subsequently rotate to a new basis where the latter matrix is also diagonal. This rotation evidently leaves g_{ij} invariant. It can be straightforwardly checked from (2.7) that, in a frame where both the metric and its first time derivative are diagonal at one instant, the subsequent evolution does not generate off-diagonal components (i.e. $\ddot{\eta}_{\alpha\beta} = 0$ for $\alpha \neq \beta$). In the diagonal frame (which will be referred to as 'Kasner frame' below), equations (2.7) become

$$\frac{\mathrm{d}}{\mathrm{d}t}\left(\Lambda t\,\frac{\dot{\eta}_{\alpha\alpha}}{\eta_{\alpha\alpha}}\right) = 0 \tag{2.9}$$

for $\alpha = 1, 2, 3$ (no summation implied). The solution to this differential equation is a simple scaling behavior

$$\eta_{\alpha\alpha}(t) = c_{\alpha}t^{2p_{\alpha}}, \tag{2.10}$$

with two integration constants. Plugging this solution in (2.6) sets $\Lambda = \sqrt{c_1c_2c_3}$ and imposes the following relation on the exponents

$$\sum_{\alpha=1}^{3} p_{\alpha} = 1. \tag{2.11}$$

It remains now to verify that this solution satisfies the constraint equations (2.2)-(2.3). Where momentum constraints (2.3) are trivially satisfied in the absence of spatial dependence, the Hamiltonian constraint (2.2) leads to an additional constraint on the exponents p_{α}

$$\sum_{\alpha=1}^{3} p_{\alpha}^2 = 1. \tag{2.12}$$

This tells us that only one of the three exponents is independent in the solution (2.10). The constraints can be elegantly solved by the introduction of a parameter $u \in [1, \infty[$:

$$p_- = -\frac{u}{1+u+u^2}, \qquad p_0 = \frac{1+u}{1+u+u^2}, \qquad p_+ = \frac{u(1+u)}{1+u+u^2}, \tag{2.13}$$

where the labels now reflect the scaling behavior of the corresponding direction instead of the numbering of the frame vectors. This parametrization illustrates that the solution to the constraints necessarily involve a non-positive, a non-negative and a positive exponent

$$-\frac{1}{3} \leq p_- \leq 0, \qquad 0 \leq p_0 \leq \frac{2}{3}, \qquad \frac{2}{3} \leq p_+ \leq 1. \tag{2.14}$$

[1] This observation is quite robust and does not change with the addition of matter. However, higher curvature corrections to Einstein gravity modify this behavior, see e.g. [11, 12].

Since $t \to 0^+$ in the approach to the singularity, one direction $(-)$ is expanding and two $(0,+)$ are contracting, while the volume of the spacelike surface decreases as (2.6).

In conclusion, we find that, near a spacelike singularity, the solution to the vacuum Einstein equations when the metric is spatially invariant is given by

$$\mathrm{d}s^2 = -\mathrm{d}t^2 + \sum_{i=\alpha}^{3} t^{2p_\alpha} (\mathrm{d}\tilde{x}^\alpha)^2 \quad \text{with} \quad \mathrm{d}\tilde{x}^\alpha = l^\alpha{}_i \mathrm{d}x^i \,, \tag{2.15}$$

with constants $l^\alpha{}_i$ (the integration constants c_α from (2.10) can be incorporated in $l^\alpha{}_i$) and where the exponents p_α are constrained by (2.11)-(2.12). This anisotropic solution describing a crunching spacetime was first derived by Kasner in 1921 [13]. One may verify that the singularity at $t = 0$ is a genuine curvature singularity, as e. g. the Kretschmann scalar $R_{\mu\nu\lambda\rho}R^{\mu\nu\lambda\rho}$ diverges at that location (the Ricci scalar is zero because the Kasner metric is a vacuum solution). Note that the isotropic Friedmann–Lemaître–Robertson–Walker metric is not compatible with the constraints (2.11)-(2.12) – matter is required for the isotropic crunch. The exponents p_α are commonly known as Kasner exponents. The frame $l^\alpha{}_i \mathrm{d}x^i$ in which both the metric and its first time derivative are diagonal defines the Kasner frame.

We now reintroduce spatial dependence in the metric $g_{ij}(\vec{x}, t)$. The key insight of BKL was to propose that, near a spacelike singularity, neglecting the three-dimensional curvature tensor ${}^{(3)}R_{ij}$ remains a good approximation during most of the evolution. The heuristic justification for this drastic simplification is the decoupling of spatial points in the vicinity of a spacelike singularity mentioned in the introduction, see Figure 1. The dynamics is ultra-local and becomes independent at every point on the spatial slice. Mathematically, this suggests that it may be a good approximation to neglect the spatial derivatives for most of the evolution. Einstein's equations then become ordinary differential equations in the time parameter that can be solved. Once a solution is found, one should then verify if (or when) this assumption breaks down. This can be done numerically or analytically by evaluating the neglected terms on the solution and verifying that they are subleading.

So, let us find a general solution to (2.2)-(2.4) with ${}^{(3)}R_{ij}$ set to zero *by hand*. This yields the evolution equations

$$\frac{\mathrm{d}}{\mathrm{d}t}\left(\sqrt{g}\kappa_i^j\right) = 0. \tag{2.16}$$

Following the same reasoning as above, one can define space-dependent Kasner axes and find that

$$\mathrm{d}s^2 = -\mathrm{d}t^2 + \eta_{\alpha\beta}(\vec{x}, t) l^\alpha{}_i(\vec{x}) l^\beta{}_j(\vec{x}) \mathrm{d}x^i \mathrm{d}x^j, \tag{2.17}$$

is a solution to (2.16), with $\eta_{\alpha\beta}(\vec{x}, t) = \mathrm{diag}(t^{2p_1(\vec{x})}, t^{2p_2(\vec{x})}, t^{2p_3(\vec{x})})$. The Kasner frame $l^\alpha{}_i(\vec{x})\mathrm{d}x^i$ locally determines the directions of contraction and expansion of spacetime on the spatial slice. Here again, the volume element decreases to zero following the profile (2.6). The geometry (2.17) is known as the generalized Kasner metric. The (now spatially dependent) Kasner exponents still obey (2.11)-(2.12). Note that the Kasner vectors are generally not proportional to total differentials. (The latter is specified using two functions of space, while a Kasner vector is characterized by three functions of space.) The Kasner frame hence does not necessarily align with the reference frame of a coordinate system [1].

Up to this point, we showed that (2.17) is a solution to the simplified Einstein equations, with (2.16) replacing (2.4). We now discuss under what conditions this elevates to an approximate

solution[2] of (2.4), where the Kasner motion continues uninterruptedly until the singularity. This question can be analyzed by evaluating the spatial Ricci tensor on (2.17) and verify whether it remains suppressed at all times as $t \to 0$. The outcome of this analysis is that the curvature terms remain subleading provided the frame vectors satisfy [1]

$$\epsilon^{ijk} l^{-}{}_{i} \partial_j l^{-}{}_{k} = 0\,, \tag{2.18}$$

where the label '$-$' refers to the notation in (2.13) and is the Kasner vector associated with the expanding direction.

We are now in a better position to address Landau's original question regarding the existence of a general solution with a singularity in GR, with the generalized Kasner solution as our best candidate. First, we need to count how many free functions of space are expected in a vacuum solution to Einstein's equations that can match arbitrary initial data. The dynamical equations (2.4) contain six second order differential equations in time for the functions $g_{ij}(\vec{x}, t)$. Hence, a general solution contains 12 arbitrary functions of the spatial coordinates. From these free functions, four are removed by the constraint equations and four can be made redundant by general coordinate invariance of the theory. We thus find that a generic solution to Einstein's equations in vacuum requires four arbitrary functions of the spatial coordinates. Is the generalized Kasner metric such a solution? A naive first counting leads to nine functions $l^{\alpha}{}_{i}(\vec{x})$ and a single independent Kasner exponent, say $p_1(\vec{x})$. However, not all these solutions satisfy the constraint equations. One can show that the momentum constraints impose three conditions on these functions [1], while the tt-constraint has already been applied to the solution to yield the constraint (2.12). In addition, one may reparameterize the coordinates x_i of the spatial slices. This allows to gauge away three more arbitrary functions of space, leaving a remainder of four functions of space specifying a generalized Kasner solution. (Note that the freedom in reparameterizing the timelike coordinate has already been exhausted by requiring the singularity to be simultaneous. This constraint fixes the integration 'constant' (2.6) to be zero.) However, we just observed that the Kasner behavior is not the complete story whenever (2.18) is not satisfied. This additional constraint removes one arbitrary function of space from the earlier counting and implies that the generalized Kasner geometry is *not* a general solution to Einstein's equations.

When (2.18) is not satisfied, the Kasner scaling behavior eventually breaks down. This occurs when certain curvature terms proportional to (2.18) become important. The intuitive picture is that the expanding direction leads to growing curvature terms. Remarkably, the effect of these terms is well understood as they usually become important only for a short amount of time. They trigger the end of the Kasner motion and the dynamics transitions into a different Kasner evolution where curvature terms are once more negligible. As we shall see, there is a formulation in which this dynamics is described by sequences of free motion interrupted by bounces against potential walls. The successive Kasner evolution is characterized by updated Kasner exponents and possibly different Kasner axes. In turn, this Kasner evolution continues until some of the curvature terms cannot be neglected any more. These will trigger the transition to yet another Kasner evolution. This process continues indefinitely, with Kasner epochs becoming shorter and shorter – measured

[2] An approximate solution is understood here to be valid to leading order in an expansion in proper time to the singularity, so that all terms in the equations of motion that would induce a change in behavior are turned off.

in proper time t – towards the singularity. The singularity becomes an accumulation point for oscillations in metric space. Any given gravity theory determines a map relating Kasner exponents before and after a bounce. This discrete dynamics encodes (some of) the chaotic properties of the near-singularity regime. For concreteness, we shall illustrate the generally expected bouncing dynamics in a simplified homogeneous setup known as the mixmaster universe, or diagonal Bianchi IX spacetime, to which we now turn.

2.2 A toy model for oscillations: the mixmaster universe

The mixmaster[3] universe is a spatially homogeneous vacuum solution to Einstein's equations in four spacetime dimensions of the form

$$\mathrm{d}s^2 = -\mathrm{d}t^2 + \eta_{\alpha\beta}(t) l^{\alpha}{}_i(\vec{x}) l^{\beta}{}_j(\vec{x}) \mathrm{d}x^i \mathrm{d}x^j, \tag{2.19}$$

with

$$\eta_{\alpha\beta}(t) = \mathrm{diag}(e^{-2\beta^1(t)}, e^{-2\beta^2(t)}, e^{-2\beta^3(t)}) \tag{2.20}$$

for some scale factors $\beta^{\alpha}(t)$, function of time only, whose evolution has yet to be determined. In the mixmaster universe, the frame vectors $l^{\alpha}{}_i$ are not arbitrary but chosen to satisfy a homogeneity condition. This condition reflects the fact that all spatial points are physically identical, which extremely simplifies the dynamics. Mathematically, homogeneous spaces are described by a symmetry group G that connects any two points $\vec{x}$ and $\vec{x}'$ by an element f of G, $\vec{x}' = f(\vec{x})$. The metric should look identical everywhere, which implies the homogeneity condition $l^{\alpha}{}_i(\vec{x})\mathrm{d}x^i = l^{\alpha}{}_i(\vec{x}')\mathrm{d}x'^i$ on the frame vectors. This condition can then be shown[4] to lead to the following constraint on the frame vectors

$$\left(\partial_i l^{\gamma}{}_j(\vec{x}) - \partial_j l^{\gamma}{}_i(\vec{x})\right) (l^{-1})^j{}_{\alpha}(\vec{x}) \, (l^{-1})^i{}_{\beta}(\vec{x}) = C^{\gamma}_{\alpha\beta}\,, \tag{2.21}$$

for some constants $C^{\gamma}_{\alpha\beta}$. Three-dimensional homogeneous geometries have been classified by Bianchi [15] and are naturally connected to Lie algebras. There exists a canonical choice for the constants $C^{\gamma}_{\alpha\beta}$, which are antisymmetric in their two lower labels from (2.21), through the structure constants of the corresponding Lie algebra. The symmetry group of interest to the mixmaster universe is $SO(3)$ – which, crucially, leads to spatial curvature – and the corresponding constants (2.21) can be chosen to be the canonical structure constants of $\mathfrak{so}(3)$ with nonzero independent coefficients $C^1_{23} = C^2_{31} = C^3_{12} = 1$. With this choice, the vectors

$$l^1{}_i \mathrm{d}x^i = \cos\psi \mathrm{d}\theta + \sin\psi \sin\theta \mathrm{d}\phi\,, \tag{2.22}$$

$$l^2{}_i \mathrm{d}x^i = \sin\psi \mathrm{d}\theta - \cos\psi \sin\theta \mathrm{d}\phi\,, \tag{2.23}$$

$$l^3{}_i \mathrm{d}x^i = \mathrm{d}\psi + \cos\theta \mathrm{d}\phi\,, \tag{2.24}$$

provide a solution to (2.21). It is a standard result in representation theory that structure constants are left invariant by

$$V^{\gamma'}_{\gamma} (V^{-1})^{\alpha}_{\alpha'} (V^{-1})^{\beta}_{\beta'} C^{\gamma}_{\alpha\beta} = C^{\gamma'}_{\alpha'\beta'} \tag{2.25}$$

[3] The term 'mixmaster' was introduced by Misner [14] in 1969, in reference to a mixing kitchen appliance that was on the market at the time.

[4] We refer to e.g. Appendix B in [8] for details.

for any orthonormal transformation V. Therefore, any rotation ${l'^{\alpha'}}_i = V^{\alpha'}_{\alpha} {l^{\alpha}}_i$ of the frame (2.22)-(2.24) solves (2.21). In the isotropic case where all β^{α}'s are equal, the spatial metric with frame vectors (2.22)-(2.24) becomes that of a three-sphere, where the Euler angles (θ, ϕ, ψ) have the usual range $0 \leq \theta \leq \pi$, $0 \leq \phi \leq 2\pi$ and $0 \leq \psi \leq 4\pi$. The three-dimensional homogeneous space corresponding to the frame (2.22)-(2.24) is known as Bianchi IX. In this section, the metric $\eta_{\alpha\beta}$ in (2.19) will be considered diagonal as in (2.20). For this reason, the mixmaster model is also known as the diagonal Bianchi IX cosmology. (The diagonal ansatz can in principle be relaxed and we will comment on the general case in section 3.3.)

The goal of this section is to analyze the dynamics of the scale factors β^{α} in the universe (2.19). Remarkably, the oscillatory dynamics that we will find is a good representative of the dynamics of inhomogeneous models [5, 6]. The mixmaster model provides a simple framework to derive the bounce law that defines the map between successive Kasner exponents – a map that will have more general applicability. Physically, the bounces originate from the spatial curvature of the homogeneous slices. As we shall see in detail in section 3, such curvature terms always lead to the same bounce law in four dimensions.

The homogeneity of the spatial slices enables one to treat any two spatial points as identical. In particular, the functions β^{α} can be chosen to only depend on time, so the dynamics is effectively one dimensional and is dictated by ordinary differential equations. (Nevertheless, the spatial derivatives of the frame vectors are essential as they induce the relevant curvature terms.) To analyze the dynamics of the scale factors, we derive Einstein's equations for the ansatz (2.19) with (2.20), projected onto the frame (2.22)-(2.24), i.e. $R^{ij} {l^{\alpha}}_i {l^{\beta}}_j = 0$. It is convenient to change time coordinate and introduce

$$\mathrm{d}\tau = \frac{\mathrm{d}t}{\sqrt{g}} = e^{\Sigma \beta^{\alpha}} \mathrm{d}t \,. \tag{2.26}$$

Towards the singularity $\tau \to -\infty$. The $\tau\tau$-direction of the Einstein equation $R_{\mu\nu} - \frac{1}{2} R g_{\mu\nu} = 0$ gives a constraint

$$f(\beta^{\alpha}(\tau), \beta^{\alpha\prime}(\tau)) = 0 \tag{2.27}$$

where the prime symbol denotes derivative with respect to τ. This simplifies the spatial equations, which yield

$$\frac{\mathrm{d}^2\beta^1}{\mathrm{d}\tau^2} = \frac{1}{2}\left(e^{-4\beta^1} - \left(e^{-2\beta^2} - e^{-2\beta^3}\right)^2\right), \tag{2.28}$$

$$\frac{\mathrm{d}^2\beta^2}{\mathrm{d}\tau^2} = \frac{1}{2}\left(e^{-4\beta^2} - \left(e^{-2\beta^3} - e^{-2\beta^1}\right)^2\right), \tag{2.29}$$

$$\frac{\mathrm{d}^2\beta^3}{\mathrm{d}\tau^2} = \frac{1}{2}\left(e^{-4\beta^3} - \left(e^{-2\beta^1} - e^{-2\beta^2}\right)^2\right), \tag{2.30}$$

while off-diagonal equations vanish identically.[5] The right-hand-side originates from the spatial Ricci curvature tensor. In the small volume limit, it is natural to consider initial conditions where all the matrix elements in $\eta_{\alpha\alpha}$ are small. (If one of them is large, it will generally roll down the potential defined by the dynamics (2.28)-(2.30).) In that case, it is a good approximation to neglect

[5] This follows directly from the diagonal assumption for $\eta_{\alpha\beta}$. For homogeneous spaces, the projected three-

the terms on the right-hand-side and the solution is

$$\beta^\alpha = a_\alpha \tau + b_\alpha . \tag{2.33}$$

This is, of course, nothing but the Kasner behavior derived in the previous section in terms of the coordinate τ, with $a_\alpha = -2\Lambda p_\alpha$. (We use the Kasner behavior of the volume (2.6) to relate τ and t via (2.26). This imposes the first constraint on Kasner exponents (2.11).) Evaluating the constraint (2.27) on this solution yields similarly (2.12). Since one of the exponents p_α is necessarily negative in order to solve the constraints (2.11)-(2.12), one of the metric components is growing or, equivalently, one of the β's is decreasing. As a consequence, the right-hand-side of (2.28)-(2.30) cannot remain suppressed indefinitely. Let us assume $p_1 \equiv p_-$ is the negative exponent. The corresponding metric component then effectively induces an exponential barrier for the three scale factors. Neglecting all the exponential terms in (2.28) but the one with β^1, one finds the bouncing solution

$$e^{-2\beta^1(\tau)} = \frac{2c_1}{\cosh 2c_1(\tau - \tau_0)}. \tag{2.34}$$

Before the bounce, the solution behaves as

$$\beta^1(\tau) \to c_1 \tau \qquad \text{for} \qquad \tau \gg \tau_0 \,, \tag{2.35}$$

such that $c_1 = -2\Lambda p_1$, since $\beta^{\alpha\prime}(\tau) = -2\Lambda p_\alpha$ during a Kasner evolution (2.33). After the bounce,

$$\beta^1(\tau) \to -c_1 \tau \qquad \text{for} \qquad \tau \ll \tau_0 \,, \tag{2.36}$$

which leads to a first relation between the initial and final Kasner regime:

$$\Lambda p_1 = -\Lambda' p_1' \,. \tag{2.37}$$

The behavior of the other scale factors β^2 and β^3 can be similarly found by explicitly solving their respective differential equations (2.29) and (2.30) with only the exponential term for β^1 turned on, evaluated on the solution for β^1 (2.34). Alternatively, since we are mainly interested here in the bounce map for the exponents, we can use that, in the current approximation,

$$\frac{\mathrm{d}^2\beta^1}{\mathrm{d}\tau^2} + \frac{\mathrm{d}^2\beta^2}{\mathrm{d}\tau^2} = 0, \qquad \frac{\mathrm{d}^2\beta^1}{\mathrm{d}\tau^2} + \frac{\mathrm{d}^2\beta^3}{\mathrm{d}\tau^2} = 0. \tag{2.38}$$

Hence, these sums of first derivatives are conserved across the bounce. We therefore find

$$\Lambda\,(p_1 + p_\alpha) = \Lambda'\,\left(p_1' + p_\alpha'\right) \qquad \text{for} \qquad \alpha = 2, 3\,. \tag{2.39}$$

dimensional Ricci tensor can be compactly written as [8]

$$2\eta R^\beta_\alpha = 2C^{\beta\gamma}\eta_{\lambda\alpha}\eta_{\mu\gamma}C^{\lambda\mu} + C^{\gamma\beta}\eta_{\lambda\alpha}\eta_{\mu\gamma}C^{\lambda\mu} + C^{\beta\gamma}\eta_{\lambda\gamma}\eta_{\mu\alpha}C^{\lambda\mu} - \eta_{\lambda\mu}C^{\lambda\mu}\left(\eta_{\alpha\gamma}C^{\beta\gamma} + \eta_{\alpha\gamma}C^{\gamma\beta}\right) + \delta^\beta_\alpha\left[\left(\eta_{\lambda\mu}C^{\lambda\mu}\right)^2 - 2C^{\lambda\mu}\eta_{\lambda\nu}\eta_{\mu\gamma}C^{\nu\gamma}\right], \tag{2.31}$$

with the matrix C related to the structure constants of the space as

$$C^\gamma_{\alpha\beta} = \varepsilon_{\alpha\beta\lambda}C^{\lambda\gamma} \tag{2.32}$$

and $\varepsilon_{\alpha\beta\lambda}$ the totally antisymmetric three-dimensional Levi-Civita symbol. For the mixmaster universe, the matrix C is the identity and the three-dimensional Ricci tensor is diagonal for $\eta_{\alpha\beta}$ in (2.20) diagonal.

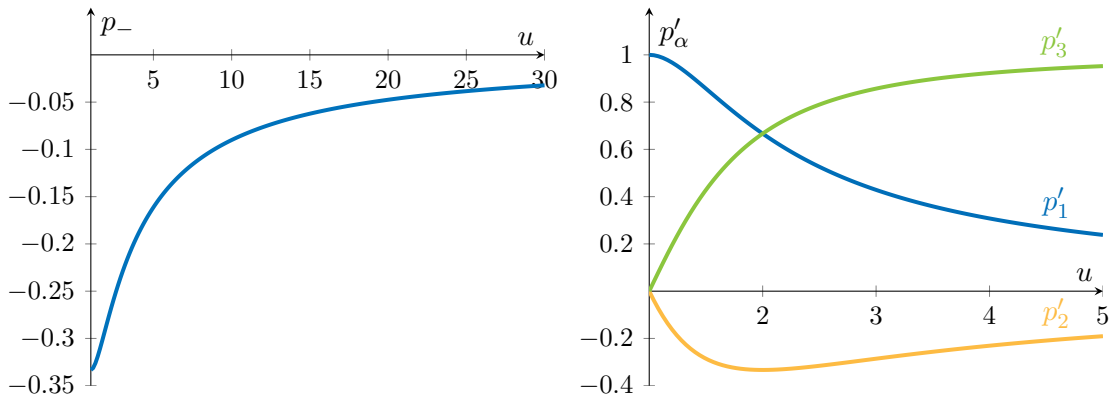

Figure 2: Left: the relation between the negative exponent and u, given by (2.13). Right: the final Kasner exponents after a curvature bounce through the map (2.42) in terms of the initial u-parameter (2.13). The main observation is that p'_2 always transitions into the expanding (negative) direction, while p'_1 is associated with the '0' or '+'-direction depending on whether $u > 2$ or $u < 2$.

Combining this with (2.37), one obtains

$$\Lambda' p'_\alpha = \Lambda\,(2p_1 + p_\alpha) \quad \text{for} \quad \alpha = 2,3 \qquad \Rightarrow \qquad \Lambda' \sum_{\alpha=1}^{3} p'_\alpha = \Lambda(3p_1 + p_2 + p_3). \tag{2.40}$$

Imposing the constraint on the sum of the Kasner exponents (2.11) on either side yields a relation between the volume scaling before and after the bounce

$$\Lambda' = \frac{\Lambda}{2p_1 + 1}. \tag{2.41}$$

Note that $\Lambda' \geq \Lambda$. Finally, using (2.37), (2.40) and (2.41) one obtains the bounce law relating initial and final exponents through the curvature terms associated with the direction β^1 in (2.28)-(2.30)

$$(p'_1, p'_2, p'_3) = \left(\frac{-p_1}{2p_1+1}, \frac{2p_1+p_2}{2p_1+1}, \frac{2p_1+p_3}{2p_1+1}\right). \tag{2.42}$$

After the bounce, the potentials in (2.28)-(2.30) are again suppressed until the terms associated with the new expanding direction triggers a new instability. This dynamics creates a never ending sequence of oscillations. The volume decreases to zero with a proportionality factor that is modified as (2.41) after each bounce.

There is a neat reformulation of the bounce law (2.42) in terms of a map for the u-parameter (2.13). For this, we assume an initial ordering $p_- = p_1$, $p_0 = p_2$ and $p_+ = p_3$. (This ordering can trivially be achieved by permuting the directions, if needed.) Remember that the expanding direction in the initial kasner evolution comes with a negative exponent p_-. This parameter takes values between $-1/3$ and 0. In terms of the parameter u, p_- is a monotonically growing function, see the left plot in Figure 2. Through the map (2.42), this expanding direction transitions into a contracting direction after the bounce. Whether the exponent associated to this frame vector afterwards takes values between $[0, 2/3]$ or $[2/3, 1]$ depends on p_-, and hence on the value of the u-parameter characterizing the initial Kasner evolution. The turnover point happens at $u = 2$ (or

$p_- = -2/7$), as shown in the right plot of Figure 2. Above (below) $u = 2$, the expanding direction turns into the contracting direction with the smaller (larger) exponent p_0' (p_+'). The direction initially associated with p_0 transitions into the expanding one irrespectively of the value of u. In addition, it is straightforward to verify using (2.13) that the relations

$$\begin{aligned} p_1' &= \frac{-p_1}{2p_1+1} = \frac{-p_-(u)}{2p_-(u)+1} = p_0(u-1)\,, \\ p_2' &= \frac{2p_1+p_2}{2p_1+1} = \frac{2p_-(u)+p_0(u)}{2p_-(u)+1} = p_-(u-1)\,, \\ p_3' &= \frac{2p_1+p_3}{2p_1+1} = \frac{2p_-(u)+p_+(u)}{2p_-(u)+1} = p_+(u-1)\,, \end{aligned} \tag{2.43}$$

and

$$\begin{aligned} p_1' &= \frac{-p_1}{2p_1+1} = \frac{-p_-(u)}{2p_-(u)+1} = p_+\left(\frac{1}{u-1}\right)\,, \\ p_2' &= \frac{2p_1+p_2}{2p_1+1} = \frac{2p_-(u)+p_0(u)}{2p_-(u)+1} = p_-\left(\frac{1}{u-1}\right)\,, \\ p_3' &= \frac{2p_1+p_3}{2p_1+1} = \frac{2p_-(u)+p_+(u)}{2p_-(u)+1} = p_0\left(\frac{1}{u-1}\right)\,, \end{aligned} \tag{2.44}$$

hold. Equipped with these observations, one finds that the map

$$u \to \begin{cases} u-1 & \text{for} \quad u > 2 \\ \dfrac{1}{u-1} & \text{for} \quad 1 < u \leq 2 \end{cases} \tag{2.45}$$

precisely encodes the bounce law (2.42) as well as the correct permutations of the directions $(-,0,+)$ in the two distinct ranges of the u-parameter. The u-map (2.45) therefore contains the same information as (2.42).

As (2.43)-(2.44) illustrate, the change of behavior of the map (2.45) as u drops below 2 signals a change in the dynamics. A generic numerical solution to (2.28)-(2.30) is depicted in Figure 3. As long as $u > 2$, the directions associated with p_- and p_0 exchange roles throughout bounces. The magnitude of the two metric components oscillate out of phase (while the third contracts) and the u-parameter decreases by one unit at every bounce. However, there necessarily comes a time where u drops below 2. This triggers a new type of oscillation where the third direction starts expanding. This point in time marks the end of a 'Kasner era'. The next bounce initiates the next Kasner era. A stretch of Kasner evolution between any two bounces defines a smaller period of time, referred to as a 'Kasner epoch'.

In section 4, we will discuss the different chaotic aspects of this dynamics in some detail. In terms of the u-map, the action $u \to u-1$ is evidently not chaotic. The second line of (2.45), however, is closely related to the well-studied chaotic discrete dynamics induced by the function $T : [0,1] \to [0,1]$,

$$T(x) = \frac{1}{x} - \left\lfloor \frac{1}{x} \right\rfloor\,, \tag{2.46}$$

called the Gauss map. It is straightforward to verify that the quantity

$$x_N \equiv (u_N \mod 1)\,, \tag{2.47}$$

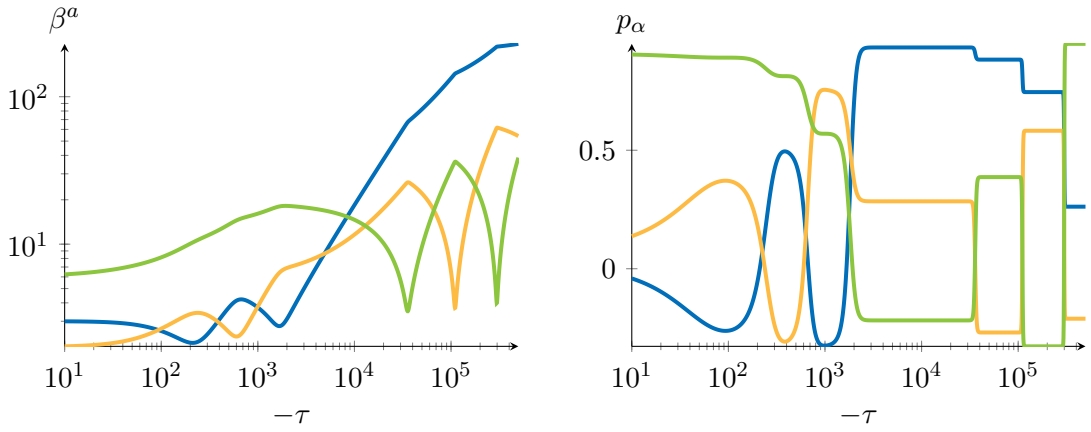

Figure 3: Left: A typical evolution of the scale factors as dictated by (2.27)-(2.30) illustrating the generic oscillatory dynamics of metric components in the vicinity of a spacelike singularity. Notice that the x-axis is $-\tau$ and we approach the singularity towards the right, with all features becoming sharp. Right: the corresponding Kasner exponents, extracted from $p_\alpha = \frac{\beta^{\alpha\prime}(\tau)}{\sum\beta^{\gamma\prime}(\tau)}$, where the primes denote derivatives with respect to τ.

in Kasner era N is mapped to the next through (2.46), i.e. $x_N = T(x_{N-1})$. The Gauss map is known to act as the right shift operator on the continued fraction expansion of a real number x in $[0,1]$

$$x = \cfrac{1}{x_0 + \cfrac{1}{x_1 + \cfrac{1}{x_2 + \cdots}}} \qquad \Rightarrow \qquad T(x) = \cfrac{1}{x_1 + \cfrac{1}{x_2 + \cfrac{1}{x_3 + \cdots}}}\,, \tag{2.48}$$

with x_i positive integers. In particular, it straightforwardly follows that for any initial u-parameter (setting initial conditions for a mixmaster evolution), one can deduce the number of oscillations in all the future Kasner eras. This data is contained in the continued fraction expansion of that single value u. The appearance of the Gauss map is a first characterization of the chaos in the near-singularity dynamics. Some of its chaotic properties will be described in section 4.1.

We conclude this section with two remarks. First, the toy model we have focused on here lacks one general feature. The Kasner frame before and after each bounce is the same. It is determined by the one-forms (2.22)-(2.24) because we chose a diagonal matrix $\eta_{\alpha\beta}$ (2.20) in our ansatz. In generic inhomogeneous setups, Kasner axes are generically found to rotate after a bounce [6]. This generic feature can in fact also be found in homogeneous geometries such as the non-diagonal Bianchi IX geometries, i.e. situations where the matrix $\eta_{\alpha\beta}$ (2.20) and its time derivative cannot be rotated simultaneously into a diagonal form at all times.[6] This setup, however, requires the addition of matter to be consistent, see e.g. [8]. We will describe the dynamics of the inhomogeneous case in section 3.3. Second, it is natural to wonder how the Schwarzschild solution fits into this narrative. The solution is integrable and does not exhibit any of the oscillations mentioned above.

[6] As we have discussed around (2.8), the metric and its first time derivative can always be diagonalized at one instant of time. However, if the diagonalization is achieved through a non-orthogonal (constant) matrix A, the corresponding transformed frame vectors $A^\alpha_\beta l^\beta{}_i \mathrm{d}x^i$ with $l^\alpha{}_i$ given by (2.22)-(2.24) will not solve (2.21) with the canonical structure constants of $\mathfrak{so}(3)$. This will then in turn lead to a non-diagonal Ricci tensor (2.31) even though η is diagonal. These off-diagonal terms, while small in the initial Kasner epoch, become larger after a bounce and lead to a rotation of the Kasner axes [5].

Nevertheless, after expanding the (e.g. planar) Schwarzschild metric in the proper time coordinate[7] near the singularity, one finds a Kasner scaling behavior, as expected. The exponents can be verified to take values $p_t = -\frac{1}{3}$ and $p_x = p_y = \frac{2}{3}$. The Schwarzschild metric therefore appears fine-tuned in the space of near-singularity solutions. There is a single Kasner epoch (no bounces) and the computed Kasner exponents lie at a corner of the allowed values (2.14).

3. Hamiltonian formalism and the billiard picture

In the first part of these notes, we analyzed the evolution of metric components in the vicinity of a spacelike singularity by solving Einstein's equations under certain assumptions that drastically simplified the dynamics. In this regime, spatially separated points decouple and the general solution describes a succession of Kasner epochs at each point in space, interrupted by exponential walls. In the $t \to 0$ limit these walls become perfectly reflective – a key point in what we will discuss next. For the specific case of the mixmaster universe, we derived the bounce law (2.42) governing the transition from one Kasner epoch to the next. In the present section, we analyze the dynamics from the Hamiltonian perspective. The Hamiltonian approach allows for an elegant reformulation of the near-singularity dynamics in terms of *cosmological billiards*. The advantage of the billiard picture was recognized in [14, 16–18], and enabled the efficient analysis of near-singularity dynamics in more complicated (supergravity) theories by Thibault Damour, Marc Henneaux, and Hermann Nicolai [19–22]. The topic of cosmological billiards is covered in great detail in the review [9].

The Hamiltonian formulation of general relativity is foundational for a canonical approach to quantum gravity. Upon canonical quantization, the Hamiltonian constraint becomes the Wheeler-DeWitt equation [23]. The solutions to this equation describe probabilities for certain metric configurations to occur on a fixed spatial slice. The Wheeler-DeWitt equation is notoriously hard to solve and is usually studied in quantum cosmology using solvable minisuperspace[8] ansätze containing only few degrees of freedom. In the present context, however, the decoupling limit of the near-singularity regime offers a well-defined setting where the equation can be solved without the need for a reduction. Moreover, the near-singularity Wheeler-DeWitt equation opens a door to the study of quantum chaos in general relativity through the quantization of the cosmological billiard model. We will come back to this in section 4.

For concreteness, we shall focus first, in section 3.1, on the derivation of the cosmological billiard for the mixmaster universe and on its canonical quantization in section 3.2. Of course, the cosmology of Bianchi IX does involve a truncation in the number of degrees of freedom since a diagonal homogeneous universe is considered. To avoid possible confusions, we shall therefore also briefly describe the cosmological billiard that emerges from the near-singularity regime of vacuum gravity in four dimensions, including inhomogeneities, in section 3.3. The cosmological billiard framework enables a concise discussion of the generic, inhomogeneous case. As we shall see, the mixmaster bounce rule (2.42) is of wide applicability and will have a major role

[7] Remember that the radial coordinate becomes timelike inside the horizon.

[8] Superspace refers here to the space of possible three-metrics. The term minisuperspace is used to denote a certain truncation in the otherwise infinite-dimensional superspace. In the context of quantum cosmology, the simplest reference to minisuperspace considers an overall homogeneous scale factor as the single dynamical degree of freedom in the theory. We refer e.g. to the Modave lectures by Caroline Jonas for more details.

in the inhomogeneous case as well. We will close in sections 3.4 and 3.5 with a discussion on the consequences of adding different types of matter and on how the billiard changes in higher dimensions.

3.1 The cosmological billiard of the mixmaster universe

The central equation of interest to us will be the Hamiltonian constraint, which reflects the time-reparameterization invariance of general relativity. This invariance is part of the larger general covariance of the theory, implying that there is no preferred time or space coordinates. The starting point of the Hamiltonian formulation of general relativity is a 3+1 decomposition of spacetime, where the freedom in redefining the time coordinate is preserved by the introduction of a lapse function that remains undetermined by the theory. In the case of the mixmaster universe, there is a natural choice of foliation where the spatial slices are the homogeneous three-spheres. For readers unfamiliar with the Hamiltonian formulation of gravity and the derivation of the constraint equations, we recommend starting with standard expositions such as [24, 25]. The Hamiltonian formulation of the BKL dynamics is covered in detail in sections 5 and 6 of [8].

To derive the Hamiltonian constraint for the mixmaster universe, we first consider the Einstein-Hilbert action for general relativity in vacuum

$$S = \int \mathrm{d}x_0\, L = \int \mathrm{d}^4x \sqrt{-{}^{(4)}g}\, R\,, \tag{3.1}$$

supplemented, in principle, by the Gibbons-Hawking-York boundary term for the initial and final slices to ensure a well-defined variational principle. For our purposes, it will be enough to consider the Einstein-Hilbert term only. As is standard in general relativity, the action generally contains second time derivatives of the metric components. Removing them using integration by parts will at the same time remove first derivatives in the lapse $n(x_0)$, which reflects the role of the lapse as a Lagrange multiplier, and not as a dynamical variable.

To express the action in terms of the Hamiltonian, we consider a foliation of spacetime analogous to (2.17)

$$\mathrm{d}s^2 = -\left(\sqrt{\eta}\, n(x_0)\right)^2 \mathrm{d}x_0^2 + \eta_{\alpha\beta} l^\alpha{}_i l^\beta{}_j \mathrm{d}x^i \mathrm{d}x^j\,, \tag{3.2}$$

where we introduced a lapse $n(x_0)$ and the frame vectors l^α are given by (2.22)-(2.24). The lapse function $n(x_0)$ will act as a Lagrange multiplier for the Hamiltonian constraint. For later convenience, we rescaled $n(x_0)^2$ by the determinant of the spatial metric $\eta = \det(\eta_{\alpha\beta})$. Note that we did not introduce a shift vector in (3.2) as we shall not be interested in the momentum constraints, which are trivial in a homogeneous setup. As in section 2.2, the metric degrees of freedom are gathered in the diagonal matrix $\eta_{\alpha\beta} = \mathrm{diag}(e^{-2\beta^1(x_0)}, e^{-2\beta^2(x_0)}, e^{-2\beta^3(x_0)})$.

Substituting (3.2) in (3.1), one obtains up to boundary terms

$$S = \int d^4x \left(n^{-1} G_{\alpha\gamma} \dot{\beta}^\alpha \dot{\beta}^\gamma - n\, \mathcal{V}(\beta^\alpha) \right), \tag{3.3}$$

with a potential

$$\mathcal{V}(\beta^\alpha) = \frac{1}{2} \sum_{\alpha=1}^{3} e^{-4\beta^\alpha} - \sum_{\alpha<\gamma} e^{-2(\beta^\alpha+\beta^\gamma)}, \tag{3.4}$$

and where the matrix G is given by

$$G_{\alpha\gamma} = \begin{pmatrix} 0 & -1 & -1 \\ -1 & 0 & -1 \\ -1 & -1 & 0 \end{pmatrix}. \tag{3.5}$$

Without the potential term, this action is a Polyakov-like action for a free massless particle in the β-configuration space. The geometry of this space is determined by the metric $G_{\alpha\gamma}$. This matrix is constant and has negative determinant. This space is therefore flat and, as we will see, Lorentzian. Let us first derive the Hamiltonian from the action (3.3). Due to the spatial homogeneity, the spatial integration in (3.3) yields a trivial volume factor. For notational convenience, we will ignore this overall factor. The action then becomes that of a conventional quantum mechanical model, whose Hamiltonian is easily computed as

$$H \equiv \sum_{\alpha=1}^{3} \pi_{\beta^\alpha} \dot{\beta}^\alpha - L \quad \text{with} \quad \pi_{\beta^\alpha} \equiv \frac{\partial L}{\partial \dot{\beta}^\alpha}, \tag{3.6}$$

such that

$$H = n\,(G^{-1})^{\alpha\gamma} \pi_{\beta^\alpha} \pi_{\beta^\gamma} + n\,\mathcal{V}(\beta^\alpha) \equiv \frac{n}{4}\,\mathcal{H}(\pi_{\beta^\alpha}, \beta^\alpha). \tag{3.7}$$

The action in its Hamiltonian form is found to be

$$S = \int \mathrm{d}x_0 \left(\sum_{\alpha=1}^{3} \pi_{\beta^\alpha} \dot{\beta}^\alpha - n\,\mathcal{H} \right). \tag{3.8}$$

The Hamiltonian constraint immediately follows by requiring invariance under variations of the lapse $n(x_0)$:

$$\frac{\delta L}{\delta n} = \frac{\delta H}{\delta n} = 0 \quad \Rightarrow \quad \mathcal{H} = 0. \tag{3.9}$$

Hence, the Hamiltonian constraint for the mixmaster universe takes the form of a sum of kinetic and potential parts

$$\mathcal{H} = \mathcal{H}_K + \mathcal{H}_P = \sum_{\alpha=1}^{3} \pi_{\beta^\alpha}^2 - \frac{1}{2} \left(\sum_{\alpha=1}^{3} \pi_{\beta^\alpha} \right)^2 + 4\mathcal{V}(\beta^\alpha) = 0. \tag{3.10}$$

In the absence of the potential, this enforces the mass-shell condition

$$\left(G^{-1}\right)^{\alpha\gamma} \pi_{\beta^\alpha} \pi_{\beta^\gamma} = 0 \tag{3.11}$$

for a massless particle moving on a null geodesic in superspace. Hamilton's equations derived from (3.7) with $\mathcal{V} = 0$ are of course consistent with this picture and tell us that $\dot{\pi}_{\beta^\alpha} = 2\partial_{x_0}(n^{-1}\dot{\beta}^\gamma G_{\alpha\gamma}) = 0$. In terms of the time variable τ (2.26), this is precisely

$$\partial_\tau^2 \beta^\alpha = 0 \tag{3.12}$$

and one recovers the Kasner behavior (2.35) and (2.36) away from the bounces. This description is the Hamiltonian picture of the Kasner epochs derived in the previous section.

We now verify the claim that the geometry on β-space is Minkowski space. For this, we introduce a different parameterization of the metric variables

$$2\beta^1 = \Omega + 2h, \qquad 2\beta^2 = \Omega - h + \sqrt{3}g, \qquad 2\beta^3 = \Omega - h - \sqrt{3}g. \tag{3.13}$$

In terms of the coordinates Ω, h and g, the Hamiltonian (3.10) takes the form

$$\mathcal{H} = -\pi_\Omega^2 + \pi_g^2 + \pi_h^2 + \mathcal{V}(\Omega, h, g) = 0, \tag{3.14}$$

with

$$\mathcal{V}(\Omega, h, g) = 2e^{-2\Omega}(e^{2h+2\sqrt{3}g} + e^{-4h} + e^{2h-2\sqrt{3}g}) - e^{-2\Omega}\left(e^{-h-\sqrt{3}g} + e^{2h} + e^{-h+\sqrt{3}g}\right). \tag{3.15}$$

Looking at the kinetic term, this set of coordinates makes the Lorentzian nature of superspace evident. The timelike coordinate Ω is related to the volume of the spacelike surface. Indeed, using (3.2) and (3.13) the local volume element is observed to be $e^{-3\Omega/2}$. The singularity is approached for $\Omega \to +\infty$ where the volume goes to zero. The identification of the volume with the timelike direction in metric space is a generic feature of gravity.

The Hamiltonian constraint encodes the fact that redefinitions of the time parameter x_0 are gauge redundancies – the theory does not fix the lapse. In the absence of a boundary, the Hamiltonian identically vanishes. Since the Hamiltonian is also the generator of time translations, evolution in x_0 is not physical but part of the gauge symmetry.[9] Instead of solving the evolution of metric components as a function of a chosen time coordinate, the Hamiltonian constraint imposes relations between metric components. The presence of a timelike direction in superspace suggests that one should interpret the volume as a 'clock', and track the evolution of the other metric components as dictated by the Hamiltonian constraint in terms of that variable.

Let us take a closer look at (3.14). The mixmaster potential (3.15) takes the form of three exponential walls and three exponential wells. The walls dominate the potential at late times, since the three wells become important in regions of metric space located behind the walls, see Figure 4. As we shall see, the wells are therefore irrelevant at late times and we shall henceforth drop them in the expression of the potential. With Ω acting as a time coordinate, we see that the locus of the walls is time-dependent – the walls are receding [14]. It is therefore convenient to perform a further change of coordinates that decouples the timelike and spacelike superspace coordinates in the exponential terms. We consider the so-called Chitre-Misner parameterization [16, 25, 27]

$$\Omega = e^{\tilde{\tau}} \cosh R, \qquad h = e^{\tilde{\tau}} \sinh R \sin\phi, \qquad g = e^{\tilde{\tau}} \sinh R \cos\phi, \tag{3.16}$$

that foliates the flat Lorentzian superspace ($\Omega > 0$) with hyperbolic 2d slices. In these variables, the Hamiltonian constraint becomes

$$\mathcal{H} = e^{-2\tilde{\tau}}\left(-\pi_{\tilde{\tau}}^2 + \pi_R^2 + \frac{1}{\sinh^2 R}\pi_\phi^2\right) + 2\sum_{i=1}^{3} e^{-2e^{\tilde{\tau}}W_i(R,\phi)} = 0, \tag{3.17}$$

[9] This is at the origin of the problem of time in quantum gravity, see e.g. [26] for a clear, concise exposition and canonical references therein for more details.

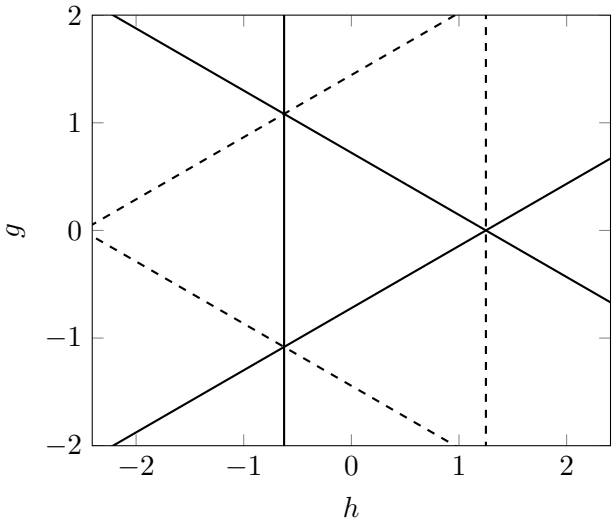

Figure 4: The locus in (h, g) space where the exponents in (3.15) vanish, for $\Omega = 1.25$. The solid lines are associated with the walls. The dashed lines represent the wells. The latter are observed to be located behind the former.

with

$$W_1(R,\phi) = -\cosh R + 2\sin\left(\phi + \frac{\pi}{3}\right)\sinh R\,, \quad W_2(R,\phi) = -\cosh R - 2\sin\phi\sinh R\,,$$
$$W_3(R,\phi) = -\cosh R + 2\sin\left(\phi - \frac{\pi}{3}\right)\sinh R\,. \tag{3.18}$$

The metric on the (R, ϕ) space can be read off from the kinetic part (3.17), and is recognized as the geometry of the Poincaré disk representation of 2d hyperbolic space. The coordinate $\tilde{\tau}$ now takes on the role of the clock and the late-time limit $\Omega \to +\infty$ is obtained as $\tilde{\tau} \to +\infty$. In this limit, the exponential potential terms turn into infinite Heaviside functions. They are either zero when $W_i(R,\phi) > 0$ or infinite when $W_i(R,\phi) < 0$. We thus find that the dynamics is constrained to the inside of a billiard in hyperbolic space with walls at $W_i(R,\phi) = 0$, for $i = 1, 2, 3$. The locus of the walls for the mixmaster billiard are geodesics on the Poincaré disk bounding an equilateral triangle and are displayed in Figure 5. The wells are subleading at late times and can be neglected.

We can now interpret the chaotic evolution derived in section 2.2 in the billiard picture. The motion described by a single geodesic segment between two walls of the billiard describes a Kasner epoch. This evolution stops when reaching a wall, bounces and turns into a new Kasner epoch. The rule dictating how to go from one set of Kasner exponents to the next follows straightforwardly from standard mirror reflection formulas. Working through this exercise for the mixmaster walls reproduces (2.42) (see e.g. [8]). We will illustrate this method when deriving the bounce rule for a different type of wall in section 3.3. Since the walls define a compact domain in hyperbolic space, the oscillatory dynamics continues forever. In the billiard picture, one Kasner era is associated to the entire span of a billiard motion between two same walls.

Note that the Hamiltonian constraint (3.10) can be solved for $\pi_{\tilde{\tau}}$. Since the variable $\tilde{\tau}$ is

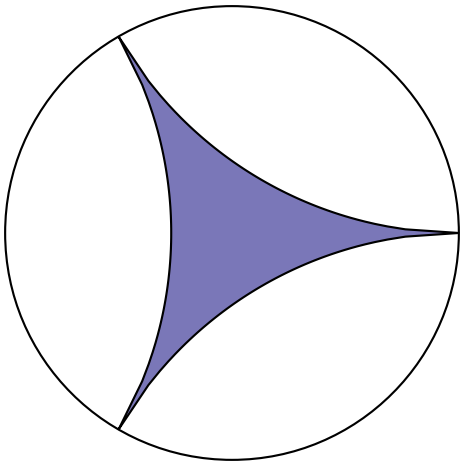

Figure 5: The cosmological billiard of the near-singularity dynamics of the mixmaster universe or diagonal Bianchi IX geometry. The walls constrain the otherwise free Kasner motion inside the equilateral triangle on the Poincaré disk (R, ϕ).

timelike, it is natural to interpret the conjugate momentum

$$\pi_{\tilde{\tau}} = \sqrt{\pi_R^2 + \frac{1}{\sinh^2 R}\pi_\phi^2 + 2e^{2\tilde{\tau}} \sum_{i=1}^{3} e^{-2e^{\tilde{\tau}} W_i(R,\phi)}}\,, \tag{3.19}$$

as a Hamiltonian. In the limit $\tilde{\tau} \to +\infty$, there is an emergent time-translation invariance and the Hamiltonian $\pi_{\tilde{\tau}}$ becomes a conserved quantity. It can be shown that the variable $\tilde{\tau}$ is a measure for the number of Kasner eras (see [28] for a derivation).

3.2 The Wheeler-DeWitt equation for cosmological billiards

The quantum chaotic properties associated to the billiards arising in gravity are quite peculiar. This will be the topic of section 4. To obtain a semi-classical description of the above Hamiltonian dynamics, we apply canonical quantization.[10] A coordinate-invariant way to quantize the momenta consists in sending

$$\sum_{A,B} \left(G^{-1}\right)^{AB} \pi_A \pi_B \to -\frac{1}{\sqrt{-G}} \partial_A \left(\sqrt{-G} G^{AB} \partial_B\right) \tag{3.20}$$

with $\left(G^{-1}\right)^{AB}$ the inverse De Witt metric that can be read from the kinetic part of the Hamiltonian. Note that we set $\hbar = 1$. The Hamiltonian turns into an operator $\hat{\mathcal{H}}$ and acts on a wavefunction for metric configurations $\Psi(\tilde{\tau}, R, \phi)$. The quantized Hamiltonian constraint is called the Wheeler-DeWitt (WDW) equation [23, 29]. For the mixmaster Hamiltonian (3.17), the WDW equation is

$$\hat{\mathcal{H}}\Psi(\tilde{\tau}, R, \phi) = \left[e^{-2\tilde{\tau}} \left(\partial_{\tilde{\tau}}^2 + \partial_{\tilde{\tau}} - \nabla_{\mathbb{H}_2}^2\right) + 2\sum_{i=1}^{3} e^{-2e^{\tilde{\tau}} W_i(R,\phi)}\right] \Psi(\tilde{\tau}, R, \phi) = 0\,, \tag{3.21}$$

[10] The classical theory of the Einstein-Hilbert action (3.1) is nonrenormalizable. This quantization procedure should therefore only be trusted in the semi-classical (or high energy) limit.

with

$$\nabla^2_{\mathbb{H}_2} = \partial_R^2 + \coth R\, \partial_R + \frac{1}{\sinh^2 R}\partial_\phi^2 \,. \tag{3.22}$$

The derivatives with respect to R and ϕ recombine into the Laplace-Beltrami operator $\nabla^2_{\mathbb{H}_2}$, the canonical Laplacian on the Poincaré disk with metric

$$\mathrm{d}s^2 = \mathrm{d}R^2 + \sinh^2 R\, \mathrm{d}\phi^2 \,. \tag{3.23}$$

To leading order in the semi-classical limit, the ordering ambiguities between coordinates and momenta in (3.21) are irrelevant. At late times, the exponential potential terms effectively turn into infinite walls and impose Dirichlet conditions on the wavefunction at the locus of the walls

$$\Psi(\tilde{\tau}, R, \phi)\ |_{W_i=0} = 0\,, \tag{3.24}$$

with $W_i(R,\phi)$ given by (3.18). The WDW equation can then simply be phrased as

$$e^{-2\tilde{\tau}}\left(\partial_{\tilde{\tau}}^2 + \partial_{\tilde{\tau}} - \partial_R^2 - \coth R\partial_R - \frac{1}{\sinh^2 R}\partial_\phi^2\right)\Psi(\tilde{\tau}, R, \phi) = 0\,, \tag{3.25}$$

with Dirichlet boundary conditions (3.24) on the walls of the hyperbolic equilateral triangle. This equation can be solved by separation of variables:

$$\Psi(\tilde{\tau}, R, \phi) = f(\tilde{\tau})\psi(R,\phi)\,. \tag{3.26}$$

Solving for $f(\tilde{\tau})$ by substituting this factorized expression into (3.25), one finds that the general solution takes the form

$$\Psi(\tilde{\tau}, R, \phi) = \sum_{n\pm} c_{n\pm}\psi_n(R,\phi)e^{\left(-\frac{1}{2}\pm i\,\varepsilon_n\right)\tilde{\tau}}\,, \tag{3.27}$$

with constants of integration $c_{n\pm}$ and where $\psi_n(R,\phi)$ solve the eigenvalue problem

$$-\nabla^2_{\mathbb{H}_2}\psi_n(R,\phi) = \left(\frac{1}{4} + \varepsilon_n^2\right)\psi_n(R,\phi)\,, \tag{3.28}$$

with boundary conditions (3.24). The eigenvalues ε_n compatible with the boundary conditions (3.24) can be shown to belong to a discrete infinite set. Solutions to this eigenvalue problem can be found by various numerical methods [30–33]. In section 4.3, we will be interested in the statistical properties of the spectrum $\{\varepsilon_n\}$ as a diagnostic for quantum chaos.

3.3 The cosmological billiard of four-dimensional vacuum gravity

For simplicity, we have focused until now on the example of the mixmaster universe, i.e. the diagonal, homogeneous Bianchi IX cosmology (2.19)-(2.20). We worked out the bounce law (2.42) from the equations of motion and derived the corresponding cosmological billiard description. While this is an interesting toy model for near-singularity oscillatory dynamics, it is not fully representative of the generic dynamics allowed by the action for pure gravity (3.1). In the language of the cosmological billiard, some walls are absent by the choice of ansatz.[11] The billiard picture

[11] This is similar to the Schwarzschild solution being a classical solution to the Einstein-Hilbert vacuum theory (3.1) while being non-generic, since the solution features a single uninterrupted Kasner evolution towards the singularity.

provides an efficient analytic approach to understand generic, inhomogeneous near-singularity physics, with additional relevant walls appearing due to the emergence of nonzero off-diagonal metric components. In fact, similar dynamics are observed in the Bianchi IX homogeneous setup whenever the diagonal condition on $\eta_{\alpha\beta}$ (2.20) is relaxed [5, 17, 18].

Let us sketch the derivation of the cosmological billiard for pure gravity in four dimensions, based on [8, 9]. As before, we assume a spatial singularity at $x_0 \to 0^+$ and consider a foliation

$$\mathrm{d}s^2 = -\left(\sqrt{g}\,n\right)^2 \mathrm{d}x_0^2 + g_{ij}(\vec{x}, x_0)\mathrm{d}x^i\mathrm{d}x^j\,, \tag{3.29}$$

with the lapse $n(\vec{x}, x_0)$ now a spatially dependent function which imposes a constraint at each spatial point. The spatial metric g_{ij} is unrestricted at this point. We will not be interested here in the momentum constraints, so we set the shift vector to zero. In deriving the Hamiltonian constraint for the inhomogeneous case, it is no longer convenient to work with Kasner frame vectors due to the phenomenon of rotation of Kasner axes mentioned at the end of section 2. Instead, we shall organize the metric degrees of freedom $g_{ij}(\vec{x}, x_0)$ in terms of new frame vectors and their corresponding scale factors β^a, using the Iwasawa decomposition [34] of the metric

$$g = \left(\mathcal{N}^T\right)\mathcal{A}\,\mathcal{N}\,, \tag{3.30}$$

where $\mathcal{A}$ is a diagonal matrix with elements $\mathcal{A}_{aa} = e^{-2\beta^a(\vec{x},x_0)}$ and

$$\mathcal{N}(\vec{x}, x_0) = \begin{pmatrix} 1 & n_1(\vec{x}, x_0) & n_2(\vec{x}, x_0) \\ 0 & 1 & n_3(\vec{x}, x_0) \\ 0 & 0 & 1 \end{pmatrix}. \tag{3.31}$$

Note that the scale factors β^a are not necessarily function of the diagonal components g_{ii} only, but rather define diagonal scale factors with respect to the frame

$$\theta^a = \mathcal{N}_i^a \mathrm{d}x^i, \tag{3.32}$$

referred to as the Iwasawa frame. Such a decomposition in terms of an upper triangular matrix is possible for any symmetric matrix and can systematically be found through a Gram-Schmidt orthogonalization procedure with respect to the inner product set by the metric, starting from the one-form $\mathrm{d}x^3$.[12] Indeed, (3.30) is equivalent to

$$\mathcal{N}\,g^{-1}\left(\mathcal{N}^T\right) = \mathcal{A}^{-1} \tag{3.33}$$

with the columns of $\mathcal{N}$ containing the coefficients of θ^a in the basis $\{\mathrm{d}x^i\}$, and the values on the diagonal of $\mathcal{A}$ are determined by the requirement that $\mathcal{N}$ has diagonal elements equal to 1. There are as many free functions appearing in g_{ij} and as there are in the Iwasawa decomposition. Since the matrix $\mathcal{N}$ has determinant 1, the local volume element is given by the scale factors $e^{-\sum\beta^a}$, as before. It is straightforward to read off the expression of the components g_{ij} in terms of β^a and n_i. These relations are easily inverted and given by

$$\begin{aligned} &\beta^1 = -\frac{1}{2}\log g_{11}, \qquad \beta^2 = -\frac{1}{2}\log\frac{g_{11}g_{22}-g_{12}^2}{g_{11}}, \qquad \beta^3 = -\frac{1}{2}\log\frac{\det g_{ij}}{g_{11}g_{22}-g_{12}^2}, \\ &n_1 = \frac{g_{12}}{g_{11}}, \qquad n_2 = \frac{g_{13}}{g_{11}}, \qquad n_3 = \frac{g_{23}g_{11}-g_{12}g_{13}}{g_{11}g_{22}-g_{12}^2}. \end{aligned} \tag{3.34}$$

[12] The decomposition is therefore non-unique and depends on the choice of coordinate system.

An important difference with the Kasner frame is that the construction of the Iwasawa frame solely uses pointwise information about the metric and does not depend on the time derivatives $\dot{g}_{ij}$. Remember that the Kasner frame is found by diagonalizing the metric and its first derivative at one instant of time, similarly to (2.8). In the absence of matter, the diagonal Kasner scaling behavior (2.17) remains valid as long as the curvature terms are negligible. When curvature terms kick in, however, a transition to a new Kasner epoch occurs and the Kasner axes may rotate. One needs to keep track of this change to describe the dynamics, and it can be shown that Kasner axes do not settle as the singularity is approached [6]. The advantage of the Iwasawa frame is that the matrix $\mathcal{N}$, while a priori time-dependent, will be found to freeze asymptotically. We will come back to this shortly. The interesting dynamics then comes primarily from the evolution of the Iwasawa scale factors β^a.

The Hamiltonian in the inhomogeneous case can be computed following steps similar to section 3.1, with the important difference that the spatial dependence is now non-trivial. Therefore, one needs to use Hamiltonian techniques for field theories instead of standard quantum mechanical systems. For conciseness, we shall state the results of the Hamiltonian computation without derivations and refer the reader to [8, 9] for details. (We shall often make reference to their terminology in order to facilitate comparison.)

The Hamiltonian form of the action (3.1) in the full vacuum theory is

$$S = \int \mathrm{d}x_0 \mathrm{d}^3x \left(\sum_{a=1}^{3} \pi_{\beta^a} \dot{\beta}^a + \sum_{a,i}^{a<i} P^i_a \dot{\mathcal{N}}^a_i - n\,\mathcal{H}(\vec{x}) \right) \tag{3.35}$$

with the momenta associated to the Iwasawa variables $\mathcal{N}$

$$P^i_a \equiv \frac{\partial \mathcal{L}}{\partial \dot{\mathcal{N}}^a_i} = \sum_{b,j} e^{2(\beta^b - \beta^a)} \dot{\mathcal{N}}^a_j \left(\mathcal{N}^{-1}\right)^j_b \left(\mathcal{N}^{-1}\right)^i_b \tag{3.36}$$

or

$$P = \mathcal{A}\dot{\mathcal{N}} \left(\mathcal{N}\right)^{-1} \mathcal{A}^{-1} \left(\mathcal{N}^T\right)^{-1} , \tag{3.37}$$

considering only the matrix elements with $a < i$ to be non-zero. The Hamiltonian density takes the form

$$\begin{aligned} \mathcal{H}(\vec{x}) &= \frac{1}{4} \sum_{a,b} (G^{-1})^{ab} \pi_{\beta^a} \pi_{\beta^b} + \frac{1}{2} \sum_{j,a,b}^{a<b} e^{-2(\beta^b - \beta^a)} \left(P^j_a \mathcal{N}^b_j\right)^2 - g\, {}^{(3)}R \\ &\equiv H_K + H_C + H_G \,, \end{aligned} \tag{3.38}$$

with G the same matrix as in (3.5), g the determinant of the spatial metric and ${}^{(3)}R$ the three-dimensional Ricci scalar. The classical equation of motion for the lapse imposes the pointwise Hamiltonian constraint $\mathcal{H}(\vec{x}) = 0$.

As in the homogeneous case, the Hamiltonian density naturally divides into kinetic and potential terms, with potential part now $H_P = H_C + V_G$. Let us discuss the different contributions in turn.

Due to the exponentials multiplying the momenta of the frame variables n_i in (3.38), their kinetic terms, collected into H_C and called centrifugal terms, behave as a potential barrier for the β-variables rather than as proper kinetic contributions in the larger configuration space (β^a, n_i).

Note that these centrifugal exponential walls are of a different type to the ones we encountered in the mixmaster universe and will therefore lead to additional billiard walls. As before, in the BKL or late-time limit, the exponential terms become infinite Heaviside functions which render their coefficients irrelevant. The Hamiltonian becomes effectively independent of the variables n_i and their conjugate momenta, which freezes these variables to constant values. This provides a heuristic understanding of the asymptotic freezing of the Iwasawa variables n_i mentioned above.

The contribution H_K only contains kinetic terms for the scale factors β^a and coincides structurally with the kinetic Hamiltonian in the homogeneous setup. Hence, the results of section 3.1 apply here as well. When the potential terms are negligible, Hamilton's equations for β^a are analogous to (3.12) and the motion follows a null ray in β^a-space

$$\beta^a = v^a \tau + \beta_0^a \,, \tag{3.39}$$

for τ an affine parameter for the geodesic motion (that can be identified with the coordinate (2.26)), $\vec{\beta}_0$ a constant vector and where the velocities satisfy a mass-shell relation due to the Hamiltonian constraint

$$\left(\sum_{a=1}^{3} v^a\right)^2 = \sum_{a=1}^{3} (v^a)^2 \,. \tag{3.40}$$

This solution is the Kasner evolution derived in the previous sections and (3.40) is equivalent to the constraint (2.12) on the Kasner exponents. (Specifically, one finds the relation $p_a = v^a / \sum v^a$ [8].) In the BKL limit, the exponential barriers become infinite Heaviside functions that impose hard wall boundary conditions on the motion when the evolution makes one of the exponents zero. The walls then induce mirror reflections in β^a-space at these locations. After a bounce on a wall with (normalized) normal vector $\vec{w}$, the velocities change according to the standard mirror rule

$$v'^a = v^a - 2\,(v \cdot w)\; w^a \tag{3.41}$$

with $v \cdot w \equiv v^a G_{ab} w^b$. Let us illustrate this formula by computing the bounce rule against one of the centrifugal walls, e.g. at $\beta^2 - \beta^1 = 0$. The normal vector is $\vec{w} = (1, -1, 0)$. Applying the mirror rule (3.41), one finds $\vec{v}' = (v^2, v^1, v^3)$ so that centrifugal walls have the simple action to exchange the values of two Kasner exponents. We will come back to this point at the end of the section. (Repeating this computation for the curvature walls at $\beta^a = 0$ can be verified to reproduce the bounce law (2.42) derived in section 2.2.)

Note that the kinetic term H_K does not receive contributions from spatial derivatives. These are all gathered in V_G, which is assumed to be negligible except at the bounces. Moreover, since the metric variables β^a originate from a pointwise Iwasawa decomposition of the metric g_{ij}, different spatial points do not influence one another through (3.38). As a result, each point undergoes independent (Kasner) null motion in β^a-space. This is the Hamiltonian perspective on ultralocality or the decoupling of spatial points near a spacelike singularity. An important consequence is that for inhomogeneous spacetimes, the spatial decoupling phenomenon leads to the emergence of an independent billiard at every point on the spatial slice.

The final term in (3.38) V_G refers to the gravitational or curvature contributions to the Hamiltonian. Among all the terms generated by the Ricci scalar, it turns out that only the exponential walls analogous to the mixmaster curvature terms (i.e. $\sim e^{-4\beta^a}$) are relevant to the billiard motion – other

terms can be discarded similarly to how the exponential wells appearing in the mixmaster Hamiltonian were found to be subdominant. In a careful analysis, one finds that the spatial derivatives of the metric inside the Ricci scalar always appear as coefficients of leading or subleading exponential walls. At late times, the behavior of interest lies in the exponentials and not in their coefficients. The only property of importance regarding the coefficients is their sign, which determines whether the exponential specifies a wall or a well. In the case of the curvature terms, their coefficients are found to be positive.

In conclusion, at late times $t \to 0$ the centrifugal and curvature walls imply respectively $\beta^b - \beta^a \geq 0$ for $b > a$ and $\beta^a \geq 0$. However, some of these constraints are implied by combinations of the other constraints. The dominant walls in the inhomogeneous case are easily determined to be

$$\beta^3 - \beta^2 \geq 0, \qquad \beta^2 - \beta^1 \geq 0, \qquad \beta^1 \geq 0\,. \tag{3.42}$$

It is an immediate feature of the billiard picture that the walls (3.42) in superspace are fixed by *linear* functions of the scale factors. By substituting the earlier superspace coordinate transformations (3.13) and (3.16) in (3.42), one finds here again a description of the near-singularity dynamics in terms of billiard motion on the two-dimensional Poincaré disk with walls now located at

$$W_1(R,\phi) = \cos\phi\,, \quad W_2(R,\phi) = -\cos\left(\phi + \frac{\pi}{3}\right)\,, \quad W_3(R,\phi) = -\cosh R - 2\sin\phi\sinh R\,. \tag{3.43}$$

The third wall is shared by the mixmaster universe. This smaller billiard is depicted in Figure 6.

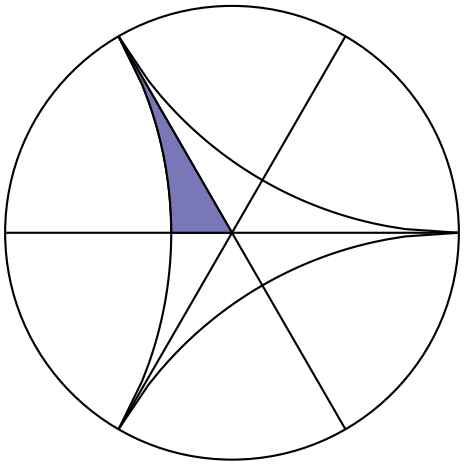

Figure 6: The cosmological billiard of inhomogeneous vacuum gravity in four spacetime dimensions on the Poincaré disk. The centrifugal walls (geometrically given by the bisections of the equilateral triangle) complement the mixmaster walls, reducing the inhomogeneous cosmological billiard to one sixth of the equilateral triangle.

Before concluding the discussion of the inhomogeneous case, it is useful to give an overview of the Lagrangian formulation of the dynamics, where the solution is usually formulated in terms of Kasner frames [5]. A notable difference is that the centrifugal walls do not appear there. In the Kasner frame, a Kasner epoch is always terminated by a curvature term that becomes large in the Ricci tensor. The key point is that the scale factors in the Iwasawa frame β^a are not the same

variables as the Kasner scale factors β^α in the Kasner frame, so there is no contradiction. This difference in perspective was pointed out in a footnote in [5], where the centrifugal potential terms in the Hamiltonian picture were termed to originate from an "inadequate choice of the axes - rotating principal axes (in [17, 18]) instead of stationary Kasner ones". (Note that [17, 18] does not consider the Iwasawa frame, but diagonalizes the metric through an orthogonal transformation. This rotation also produces centrifugal terms.) It is instructive to understand the origin of the permutation of the Iwasawa exponents – due to centrifugal terms in the Hamiltonian picture of the Iwasawa frame – from the perspective of the Kasner frame. To this end, we focus on a complete stretch of Kasner evolution *in the Kasner frame* (i.e. assuming no curvature bounces) and track the evolution of the Iwasawa variables. Consider first the spatial metric expressed now in the Kasner frame

$$g_{ij} = \eta_{\alpha\beta}(\vec{x}, t) l^\alpha{}_i(\vec{x}) l^\beta{}_j(\vec{x}) \,, \tag{3.44}$$

with $\eta_{\alpha\beta}(\vec{x}, t) = \text{diag}(t^{2\mathbf{p}_1(\vec{x})}, t^{2\mathbf{p}_2(\vec{x})}, t^{2\mathbf{p}_3(\vec{x})})$, where we momentarily use boldface typesetting to differentiate the 'Kasner' exponents $\mathbf{p}_\alpha$ from the 'Iwasawa' Kasner exponents p_a. We can then use the relations (3.34) with (3.44) to express the Iwasawa variables in terms of the Kasner variables. For instance, the first Iwasawa scale factor becomes

$$\beta^1 = -\frac{1}{2} \log \sum_{\alpha=1}^{3} t^{2\mathbf{p}_\alpha} \, (l^\alpha{}_1)^2 = v^1 \tau + \beta_0^1 \tag{3.45}$$

with $v^a = -2\Lambda p_a$. The key takeaway is that the different terms in (3.45) can dominate at different times along the Kasner evolution. In figure 7, we illustrate the time dependence of the Iwasawa scale factors β^a during a full Kasner evolution (no curvature bounce) for a randomly generated matrix $l^\alpha{}_i$. We observe that the centrifugal bounces for the scale factors β^a in the Iwasawa frame originate from the exchange in domination of the various Kasner scale factors in the expression for the Iwasawa scale factors during a single Kasner epoch in the frame (3.44). Moreover, the right panel in Figure 7 shows that the Iwasawa frame is approximately constant between centrifugal bounces. We mentioned above that the Iwasawa frame is useful in the Hamiltonian formalism because of its asymptotic freezing properties. To be specific, the advantage of the Iwasawa frame is that their late time value in each full Kasner evolution [9]

$$n_1 \to \frac{l^1{}_2}{l^1{}_1} \,, \quad n_2 \to \frac{l^1{}_3}{l^1{}_1} \,, \quad n_3 \to \frac{l^1{}_1 l^2{}_3 - l^1{}_3 l^2{}_1}{l^1{}_1 l^2{}_2 - l^1{}_2 l^2{}_1} \,, \tag{3.46}$$

remains unaltered after a curvature bounce. (Note that (3.46) uses the convention that $\mathbf{p}_1 < \mathbf{p}_2 < \mathbf{p}_3$ and that the vectors $l^\alpha{}_i$ with fixed α are normalized.) More precisely, substituting the known rotation rules for the Kasner axes $l^\alpha{}_i \to l'^\alpha{}_i$ after a curvature bounce in conjunction with (3.34) before and after the bounce shows that the limiting values $n_i \to n_i'$ (see [9] section 5.3 for a derivation). This is a more precise sense in which the Iwasawa frame freezes asymptotically. In contrast, while the metric is, by definition, initially diagonal in the Kasner frame, off-diagonal terms generically develop after curvature bounces [5] causing Kasner axes to rotate.

3.4 Some effects of matter

In their seminal paper on cosmological billiards [9], Damour, Henneaux and Nicolai review the derivation of the billiard description for any Einstein-dilaton-p-form system near a spacelike

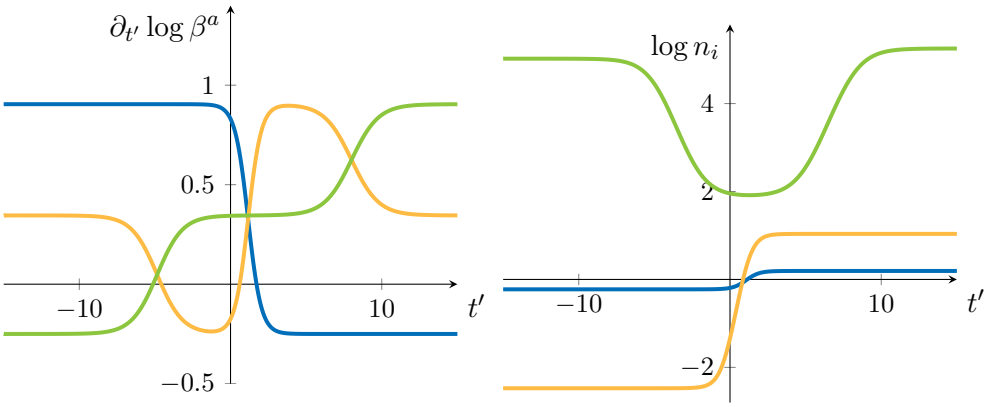

Figure 7: Left: the time evolution of the Iwasawa scale factors β^a (β^1 in blue, β^2 in yellow and β^3 in green) during a Kasner epoch with $\mathbf{p}_1 = -0.25$ and a randomly generated matrix $l^\alpha{}_i$ (selected such that the centrifugal bounces are well separated for clarity). The other two Kasner exponents are found by solving the constraints (2.11) and (2.12) and take values $\mathbf{p}_2 \approx 0.345$ and $\mathbf{p}_3 \approx 0.905$. For visualization purposes, we plot $\partial_{t'} \log \beta^a$ against t' with $t = e^{-t'}$, as a proxy for the Iwasawa exponents p_a. During this evolution, one first observes the Iwasawa β^2 and β^3 exchange their scaling behavior. In the Hamiltonian picture, this corresponds to a bounce against the wall at $\beta^3 - \beta^2 = 0$. Next, we observe a bounce against $\beta^2 - \beta^1 = 0$ and a final bounce against $\beta^3 - \beta^2 = 0$. Right: the corresponding evolution of the Iwasawa frame functions n_i.

singularity in D dimensions. Without the billiard picture, one would have to analyze the coupled equations of motion in the decoupled limit, as we did in section 2. The billiard approach, on the other hand, provides an intuitive and efficient way to incorporate the consequences of a coupling to matter. For the purpose of these notes, we illustrate some of the different effects matter can induce by focusing on just two examples, the scalar field and a vector field, and refer to the review [9] for a systematic Hamiltonian study of Einstein-dilaton-p-form systems.

The major difference between a scalar and a vector field is the fact that the vector field has indices, and hence naturally multiplies metric components in the Hamiltonian, while the scalar field does not. Specifically, the conjugate momentum to the scalar field appears in the following way in the Hamiltonian constraint:

$$\mathcal{H} = -\pi_\Omega^2 + \pi_g^2 + \pi_h^2 + \pi_\Phi^2 + \mathcal{V}(\Omega, g, h, \Phi) = 0\,. \tag{3.47}$$

The potential $\mathcal{V}$ may depend on Φ, through the addition of a scalar potential to the Lagrangian. A nontrivial scalar field therefore effectively increases the dimension of the cosmological billiard by one unit. If the scalar field is free, the additional billiard direction is unrestricted and chaotic oscillations are not generic. Scalar fields can thus eliminate BKL chaos.

In contrast, the momenta conjugate to the components of a vector field couple to the metric in the Hamiltonian. Schematically, we write

$$\mathcal{H} \equiv -\pi_\Omega^2 + \pi_g^2 + \pi_h^2 + g_{ij}\pi^i\pi^j + \mathcal{V}(\Omega, g, h, A) = 0\,, \tag{3.48}$$

with π^i the momenta conjugate to the spatial components of the vector field. See [28, 35] for examples. Due to the coupling to the metric, the vector fields therefore contribute to the potential part of the Hamiltonian instead of the kinetic terms. This is quite similar to the classification of the

momenta of off-diagonal metric components as potential instead of kinetic terms in (3.38). Vector fields define additional potential walls that may dominate over some of the curvature and symmetry walls from the gravitational action and may thus modify the boundaries of the relevant cosmological billiard. For completeness, we note that additional care is needed in the case of massive vector fields due to the longitudinal mode behaving like a scalar [35]. When using an ansatz where the longitudinal mode is fixed to zero, we recover the situation exposed here.

3.5 Cosmological billiards in higher dimensions

Scalar(-like) degrees of freedom and the diagonal metric scale factors determine the dimensionality of the cosmological billiard. In the Iwasawa frame, the off-diagonal metric components freeze asymptotically and contribute solely to the shape of the billiard by defining additional walls. Therefore, repeating a near-singularity analysis as in section 3.3 in D-dimensional pure gravity produces a cosmological billiard of dimension $D-2$. Every additional scalar degree of freedom in the theory should increase this dimension by one.

A surprising feature of Einstein's equations is the fact that, in spacetime dimensions higher than $D = 10$, the generalized Kasner asymptotic solution is stable and can, in fact, continue forever. Specifically, there is an open set of Kasner exponents for which curvature terms never become large. In these dimensions, oscillations are expected not to be generic any more as it has been argued that the dynamics usually reaches such a generalized Kasner solution after a few bounce [36, 37]. However, matter can and does modify this behavior in some cases. Remarkably, the addition of a 3-form, which appears in the bosonic sector of maximal supergravity, reinstates chaos in eleven dimensions. Precisely in $D = 11$, the ingredients of the theory conspire so that the corresponding billiard is chaotic and moreover displays the peculiar arithmetic properties that we will touch upon in section 4.3. The existence of oscillatory dynamics has been investigated in higher-dimensional theories of gravity and supergravity in [19, 20, 36, 37].

To conclude, we highlight an intriguing connection between cosmological billiards and infinite dimensional Lorentzian Kac-Moody algebras (KMAs). As pointed out above, the location of the billiard walls that we encountered are specified by linear functions of the scale factors. It turns out that the dominant walls of most physically interesting theories can be identified with the simple roots of some Lorentzian KMA. More specifically, the reflection group through the walls of these cosmological billiard is identical to the Weyl group of the corresponding Lorentzian KMA. The rank r of the algebra relates to the dimension d of the billiard as $r = d + 1$. As a matter of example, the Kac-Moody algebra corresponding to the billiard of four-dimensional pure gravity with walls (3.42) is A_1^{++}. When the volume of the billiard is finite, the dynamics shows never-ending oscillations, and the corresponding KMA is of the hyperbolic type. A remarkable fact is that there are no hyperbolic KMAs of rank higher than 10 [38, 39]. Moreover, the three types of billiards associated with the KMAs of rank 10 are all realized in string theories [21, 40]. This coincidence may suggest a hidden role for these algebraic structures in the symmetries underlying gravitational theories, see [39] for a review on this topic. This connects with other conjectures that relate the exceptional group E_{10} to eleven-dimensional supergravity.

4. Quantum chaos in cosmological billiards

The hyperbolic billiards for the mixmaster universe and pure gravity share a distinctive feature. They are arithmetic triangles. Put differently, their surface is identified with the fundamental domain of an arithmetic group. For these specific cases, the arithmetic groups are (related to) subgroups of the modular groups $PSL(2,\mathbb{Z})$. This characteristic has many number theoretic implications. The best known example is that their level spacing statistics – a spectral diagnostic for quantum chaos – is anomalous. In this section, we give a broad overview of the chaotic properties of the cosmological billiards. We start by reviewing some aspects of the description of chaos associated with the classical oscillatory behavior near the singularity in section 4.1. Whether or not the mixmaster dynamics is classically chaotic was heavily discussed in the 80s [41]. We will give a brief account of some of the main arguments (see also [42]). The remaining sections 4.2-4.4 revolve around quantum chaos in arithmetic triangles. In section 4.2, we give a brief primer on spectral probes of quantum chaos. In section 4.3, we review the properties of these probes in arithmetic triangles and we close with a discussion of the emergence of arithmetic chaos in gravity and string theories in section 4.4.

4.1 Classical chaos in cosmological billiards

There is no single definition of classical chaos. Nonetheless, it is widely agreed upon that chaotic dynamical systems should exhibit some form of sensitivity to initial conditions. A quantitative description of this feature is the exponential divergence in the evolution of nearby points in phase space. The rate of divergence defines the Lyapunov exponent

$$\lambda = \lim_{t\to+\infty} \lim_{\delta x_0 \to 0} \frac{1}{t} \log \frac{||\delta x_t||}{||\delta x_0||} \tag{4.1}$$

where δx_0 is the initial separation between two points in phase space and δx_t is their separation after some time t has elapsed. This exponent depends on the choice of the two initial phase space points. The Lyapunov exponent characterizing the system is usually obtained by considering the maximal exponent averaged over phase space [43]. We point out that two ingredients in (4.1) are of importance in the description of Lyapunov exponents. The first is the distance measure on phase space and the second is the time variable t appearing in the definition. In the context of the mixmaster dynamics, or more general gravitational dynamics, a good choice for both these components is far from straightforward.

Let us first discuss the distance measure. Although there is a natural, coordinate-invariant distance measure on the space of spatial metrics in terms of the De Witt metric, the signature is Lorentzian. As a result, trajectories may have zero length in this measure and this leads to ill-defined Lyapunov exponents. Initial efforts in describing the classical mixmaster chaos hence rather opted for the use of a Euclidean flat metric, as is standard in conventional Hamiltonian systems. However, this distance measure is not invariant under general reparameterization of the metric variables and it is unclear what to make of a gauge-dependent Lyapunov exponent.

The second ambiguity concerns the time variable t multiplying the Lyapunov exponent. Standard dynamical systems come with a preferred or absolute time specifying the evolution. This is not the case in the mixmaster dynamics, since general relativity is a time-reparameterization invariant

theory. During our discussions in section 2 we encountered at least two different times, the proper time t and the variable τ (2.26). These two different parameterizations are exponentially related, so it is evident that chaos could be signaled by a positive exponent through the use of one of them, while being seemingly absent in the other. This expectation was confirmed by numerical studies of Lyapunov exponents in the mixmaster universe for these different choices of time [44–49]. Works using the proper time t suggest chaotic behavior with positive Lyapunov exponent, but have the caveat that one cannot take $t \to \infty$ as required by the definition (4.1) since the singularity is at $t = 0$. In terms of the variable τ (2.26) the Lyapunov exponent is found to tend to zero towards the singularity [44]. The physical difference between these two times is evidently that the oscillations accumulate towards $t \to 0$ in proper time, while they get stretched out in terms of the variable τ as $\tau \to -\infty$, as in Figure 3. These two examples illustrate that Lyapunov exponents are ambiguous in time-reparameterization invariant theories and other probes should be used.

A clear sign of chaos in the classical dynamics is provided by the emergence of the Gauss map (2.46) in the asymptotic transformation of Kasner exponents between eras.[13] The Gauss map can be shown to be sensitive to initial conditions, ergodic and mixing [41] (see also [50]). In fact, these results preceded the computations of the Lyapunov exponent in the continuous dynamics [44–49] by a decade. For a discrete map f, Lyapunov exponents are defined according to [43]

$$\sigma = \lim_{N\to\infty} \frac{1}{N} \log \left| \frac{\mathrm{d}f^N(x_0)}{\mathrm{d}x_0} \right| . \tag{4.2}$$

In numerical simulations, it is important to send $\mathrm{d}x_0 \to 0$ faster than $N \to \infty$ in order to probe the rate of exponential growth. The averaged Lyapunov exponent is positive for the Gauss map. One can moreover show that the memory of initial conditions is washed away in an order 1 number of eras.

Recall that the Gauss map (2.46) only encodes the *chaotic* part of the u-map (2.45). In particular, one loses information about the past evolution if the only data we keep track of are the values x given by (2.47). By a change of parameter $x' \equiv 1/u$, one can reformulate the chaotic and nonchaotic parts in terms of another map defined on the interval $[0, 1]$. This map is called the Farey map. The dynamics of this map is organized around a self-similar fractal strange repellor [51]. This constitutes a gauge-invariant characterization of the mixmaster chaos.

The billiard picture offers yet another compelling perspective on the chaotic nature of the dynamics. Single-particle dynamics on closed two-dimensional hyperbolic domains is a textbook example of classical chaotic motion [52]. The first time a proof of ergodicity could be formulated in a dynamical system [53] was, in fact, for the hyperbolic billiard relevant to pure gravity in four dimensions, shown in Figure 6. The strong sensitivity to initial conditions is due to the combined effect of the hyperbolic geometry, which naturally drives geodesics apart, and the presence of the walls that lead to mixing and ergodicity [54]. We remark that these last two points of view are an exact description of the dynamics only in the hard-wall BKL limit.

[13] It is also interesting to note that one can make direct contact with the discrete u-map by constructing a *continuous* time variable that evolves only when the free part of the Hamiltonian constraint is not zero, i.e. it evolves only during bounces [47]. This time variable is called the minisuperspace (MSS) proper time.

4.2 Quantum chaos from spectral statistics

We now turn to the chaotic properties of the Wheeler-DeWitt equation near the singularity. A naive translation of the sensitivity to initial conditions to quantum mechanics is generally complicated by the Heisenberg principle, since the very concept of a trajectory at given initial momentum and position loses its meaning in the quantum realm. While there are correlators designed to probe this sensitivity (such as the OTOC [55]), we have seen that even at the classical level it is hard to make good use of this notion of chaos in time-reparameterization invariant theories.

Another popular diagnostic of quantum chaos was introduced by Wigner. He was interested in characterizing the spectrum of atoms, and observed universality in the statistics of spacings between neighboring energy eigenvalues [56, 57]. The level spacings were found to closely follow the blue curve in Figure 8, now known as the Wigner-Dyson surmise. Bohigas, Giannoni and Schmit [58]

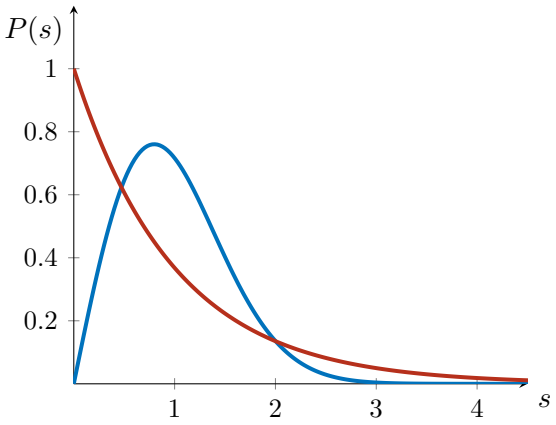

Figure 8: The expected level spacing statistics of (time-reversal invariant) chaotic versus integrable models, following respectively the Wigner-Dyson surmise (4.3) (blue) or the Poisson distribution (4.4) (red).

later conjectured that models with a classically chaotic limit feature energy spectra with spacings[14] consistent with the Wigner-Dyson surmise

$$P(s) = \frac{s\pi}{2} e^{-\frac{\pi s^2}{4}}. \tag{4.3}$$

(This curve assumes time-reversal invariance of the model. Similar distributions exist for other symmetry classes [61].) A key feature of (4.3) is the polynomial decay at low spacings, meaning that energy levels tend to repel in chaotic models. On the other hand, one expects the energy levels in generic integrable models to be largely uncorrelated – due to the hierarchy of symmetry sectors generated by the conserved charges. The level spacing statistics of integrable models is then expected to follow a Poisson distribution

$$P(s) = e^{-s}, \tag{4.4}$$

displayed as the red curve in Figure 8.

[14] We note that the energy levels first need to be appropriately rescaled to remove the non-universal influence of the energy density. This process is referred to as 'unfolding', see e.g. [59, 60].

Other generic properties of quantum systems can be found in long-range correlations between energy eigenvalues. Some of these correlations can be diagnosed by the spectral form factor (SFF) $K(t)$, which is the Fourier transform of the two point correlation function of the level density $d(E)$.[15] If one is able to compute (part of) the spectrum of a quantum model numerically or analytically, the corresponding spectral form factor can be analyzed using the formula

$$K(t) = \frac{1}{N} \sum_{n,m=1}^{N} e^{-i(E_n - E_m)t} \,. \tag{4.5}$$

Some degree of control can be acquired on the SFF by use of periodic orbit theory [62–64], where one uses periodic orbits of the classical limit to infer information about the level density of the quantum system. For chaotic systems, the SFF is expected to feature the characteristic slope, dip, linear ramp and plateau behavior [63, 65, 66], in analogy to random matrix theory ensembles. The shape of the slope is system dependent and the plateau follows from discreteness and the generic absence of degeneracies in chaotic spectra.[16] The shape of the ramp is related to spectral rigidity, or long-range repulsion. In chaotic systems, one expects a linear ramp whose prefactor depends on symmetries such as time-reversal invariance. For generic integrable systems, the spectrum should be largely uncorrelated and this leads to a SFF that quickly reaches a plateau value, on time scales of the order of the shortest classical orbit period.

4.3 Arithmetic quantum chaos

Arithmetic triangles are special. Their level spacing statistics is of a particular type and they can be argued to be a counter example to the BGS conjecture. The origin of their difference with generic models is, however, very well understood as we now discuss.

The spectrum of hyperbolic billiards is discrete, determined by eigensolutions of the hyperbolic Laplacian with specified boundary conditions, see (3.18) for the mixmaster universe and (3.43) for pure gravity. Such spectra can be computed numerically [30, 31]. For the two billiards derived above, a histogram of their level spacing statistics surprisingly reveals approximate Poisson statistics [67], even though the classical dynamics is ergodic. The origin of the anomalous statistics can be traced back to the particular arithmetic properties of these hyperbolic billiards [10, 68, 69]. The aim of this section is to highlight the peculiarities of the model that lead to the anomalous statistics. We will, however, keep this discussion purposely short. Details and derivations can be found in [10]. Arithmetic quantum chaos was the topic of a separate set of lectures [70] and lecture notes will soon be available.

The arithmetic features of the billiard become most apparent when going to the upper half plane description of 2d hyperbolic space, introducing coordinates $(\tilde{\tau}, x, y)$

$$\beta^1 = \frac{e^{\tilde{\tau}}}{\sqrt{2}} \frac{x}{y} \,, \qquad \beta^2 = \frac{e^{\tilde{\tau}}}{\sqrt{2}} \frac{1-x}{y} \,, \qquad \beta^3 = \frac{e^{\tilde{\tau}}}{\sqrt{2}} \frac{x(x-1)+y^2}{y} \,, \tag{4.6}$$

[15] Given a quantum mechanical spectrum of energies $\{E_n\}$, the level density is $d(E) = \sum_n \delta(E - E_n)$.

[16] There may be degeneracies due to global symmetries. However, the level spacing statistics analysis should be performed independently in blocks of fixed quantum numbers, which usually removes those degeneracies.

with $y > 0$. On the upper half plane, the hyperbolic Laplacian (3.22) and the corresponding eigenvalue problem (3.28) take the form

$$\nabla^2_{\mathbb{H}_2}\psi_n(x,y) = y^2\left(\partial_x^2+\partial_y^2\right)\psi_n(x,y) = -\left(\frac{1}{4}+\varepsilon_n^2\right)\psi_n(x,y)\,, \tag{4.7}$$

with the boundaries of the cosmological billiards located at

$$x=0, \qquad x=1 \qquad \text{and} \qquad \left(x-\frac{1}{2}\right)^2+y^2=\frac{1}{4} \qquad \text{(mixmaster)} \tag{4.8}$$

$$x=0, \qquad x=\frac{1}{2} \qquad \text{and} \qquad x^2+y^2=1 \qquad \text{(pure gravity)} \tag{4.9}$$

These two billiards are depicted in Figure 9. The key feature of these surfaces, is that they precisely

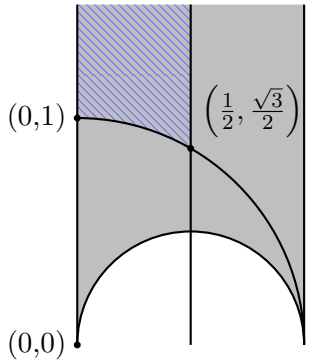

Figure 9: The cosmological billiard for the mixmaster universe (gray) and inhomogeneous pure gravity (purple) drawn on the upper half plane representation (x, y) of $\mathbb{H}_2$.

coincide with half of the fundamental domain[17] of a subgroup of the modular group

$$PSL(2,\mathbb{Z}) = \left\{\begin{pmatrix} a & b \\ c & d\end{pmatrix} \mid ad-bc=1\right\}, \tag{4.10}$$

where matrices identical to one another up to an overall minus sign are identified. The subgroup of interest to the mixmaster universe is the principal congruence subgroup of the modular group

$$\Gamma(2) \equiv \left\{\begin{pmatrix} a & b \\ c & d\end{pmatrix} \in PSL(2,\mathbb{Z}) \mid (a,d=1 \wedge b,c=0) \mod 2\right\}, \tag{4.11}$$

while, in the case of pure gravity, the relevant arithmetic group is the modular group itself.

Classical dynamics on these surfaces have an unusual feature with direct implications on the quantum energy spectrum. There is a one-to-one correspondence between periodic orbits on the billiard surface and the (hyperbolic) conjugacy classes of the associated arithmetic group (4.10) or (4.11). One can moreover show that the lengths of the closed orbits are computed by the trace of the elements in the corresponding conjugacy class. The lengths therefore take values in a discrete set,

[17] A surface defines a fundamental domain for a group G if every point outside of the surface is mapped inside by some element of G and if no two points in the surface are related by a nontrivial element of G.

since the matrices have integer trace. A common feature of chaotic models is their exponentially growing number of geodesics of length below a certain threshold. For arithmetic billiards, these two properties combined enforce the length spectrum to have a huge number of (exact!) degeneracies that grows exponentially with the length. (Generic chaotic systems display no more than an order one number of closed orbits of exactly the same length.) By use of periodic-orbit theory, it has been understood that this exponential degeneracy produces an exponential ramp in the spectral form factor, instead of the usual linear ramp [10, 69]. As a result, the SFF reaches saturation much faster than in ordinary chaotic models, with a time of saturation tending to zero at high energies. This is consistent with uncorrelated levels, leading to the observed Poissonian level spacing statistics in the high energy part of the spectrum [10, 67, 71].

The relation of the billiard surface to the modular domain has far more implications than solely constraining correlations in the spectrum. Even though common spectral probes fail to diagnose chaos in arithmetic triangles, the energy eigenfunctions do seem to exhibit signs of randomness and even suggest connections to random matrix theory. To illustrate this, we consider the following expansion in Fourier modes of the Laplacian

$$\psi_n(x,y) = \sum_{m=1}^{\infty} c_m^n \sqrt{y} K_{i\varepsilon_n}(2\pi m y)\sin(2\pi m x), \tag{4.12}$$

with undetermined coefficients c_m^n and energy ε_n and where $K_{i\varepsilon_n}$ is the modified Bessel function of the second kind. These modes are solutions to the Laplacian eigenvalue problem (4.7) with energy ε_n and solve the first two boundary conditions in (4.9) for any combination of c_m^n and ε_n. However, only for discrete values of ε_n can one find corresponding coefficients c_m^n such that (4.12) also satisfies the third boundary condition in (4.9). The resulting Fourier coefficients c_m^n are found to obey very constraining relations. These relations follow from the existence of an infinite family of operators that mutually commute and commute with the Laplacian and the boundary conditions,[18] called Hecke operators T_n with $n \in \mathbb{N}$. (The existence of an infinite tower of conserved quantities may be disturbing since the model is not integrable. It is important to realize though that there is no classically conserved charges associated to these operators. Nevertheless, the construction of the Hecke operators is closely related to the classical periodic orbits [10, 71].) The Hecke operators can be shown to satisfy the following multiplicative property (see e.g. [72])

$$T_n T_m = \sum_{d|(n,m)} T_{\frac{nm}{d^2}} \tag{4.13}$$

where the sum runs over all divisors d of the greatest common divisor of n and m. Since the Hecke operators commute with the Laplacian,[19] they have a diagonal action on the solutions to the eigenvalue problem. The eigenfunctions of arithmetic triangles are therefore joint eigenvectors of both the Laplacian and an infinite set of Hecke operators. The key point now is that the Fourier coefficients c_m^n can be shown to be the eigenvalue of T_m for the eigenfunction ψ_n. The multiplicative property of the operators (4.13) is thus immediately transferred to the Fourier coefficients c_m^n.

[18] Commuting with the boundary conditions is understood here as mapping the space of wavefunctions that respect the boundary conditions to itself. The form of the Hecke operators hence depends on the shape of the triangle.

[19] The spectrum of the Laplacian with boundary conditions (4.9) is not expected to have degeneracies.

Solutions to the billiard eigenvalue problem hence have Fourier coefficients constrained by the Hecke relations

$$c_n^k c_m^k = \sum_{d|(n,m)} c_{\frac{nm}{d^2}}^k \,. \tag{4.14}$$

In particular, it follows from the unique prime decomposition of natural numbers and (4.14) that all c_n^k, at fixed k, can be obtain from the coefficients c_p^k, with p prime, through (4.14). The primed coefficients therefore define the independent data of a wavefunction. Various theorems controlling the statistical behavior of the primed coefficients have been conjectured. For instance, the Ramanujan-Petersson conjecture states that, after normalizing $c_1^n = 1$, the primed coefficients take values in a finite range

$$|c_p^n| \leq 2 \qquad \forall p \in \mathbb{P}, n \in \mathbb{N}_0 \,. \tag{4.15}$$

At a fixed energy ε_n, the distribution of primed coefficients of the corresponding wavefunction are moreover expected to follow a semi-circle, which may suggest a connection to random matrix theory. This is known as the Sato-Tate conjecture. This conjecture has been extensively tested for the modular group [32, 33].

4.4 String theories, M-theory and their relation to octonions

At first, the emergence of arithmetic triangles in the near-singularity dynamics may appear accidental. Indeed, there are many variations of matter content and spacetime dimensions one could consider, and these choices may modify the shape of the cosmological billiard. The resulting billiard does not necessarily exhibit arithmetic chaos – or even generic chaos. (Note that, at least for two dimensional hyperbolic surfaces, all the arithmetic triangles have been classified [73], see also appendix E of [10].) This fact is usually overshadowed by the mixmaster universe and the four-dimensional pure gravity setup that are commonly put forward when introducing the work of BKL. However, as we discussed in section 3.5, it is an intriguing coincidence that the generalized Kasner solution becomes stable for theories in dimensions higher than 10, and that the matter content of eleven dimensional supergravity is precisely such that chaos is reinstated.

Furthermore, there is an interesting mathematical connection between the Weyl groups of hyperbolic Kac-Moody algebras of ranks 3, 4, 6 and 10 and modular groups over integers in the four normed division algebras $\mathbb{K} = \mathbb{R}, \mathbb{C}, \mathbb{H}$ and $\mathbb{O}$ [74, 75]. We have just discussed how the cosmological billiard of pure gravity in four dimensions can be identified with half of the fundamental domain of the modular group $PSL(2, \mathbb{Z})$. It was shown in [74] that a connection of this sort exists between generalizations of the modular group, where the matrices are defined over integer lattices related to the other three normed division algebras, and more complicated gravitational theories whose cosmological billiard is related to higher rank hyperbolic Kac-Moody algebras. Among the hyperbolic KMAs of rank 10, the algebra E_{10} stands out for several reasons. One of them is the fact that all simply laced hyperbolic Kac–Moody algebras can be embedded into E_{10} [76]. Moreover, E_{10} is the algebra of relevance to maximal supergravity and M-theory [21]. Through the correspondance put forward in [74, 75], the Weyl group of E_{10} is related to the generalized modular group over integers in the octonions $\mathbb{O}$. Because of the connection to these generalized modular groups, the near-singularity dynamics in all such gravitational theories feature arithmetic chaos. These observations may therefore suggest a more fundamental role for arithmetic symmetry in

gravity [21, 39], and possibly quantum gravity. Recently, systematic number-theoretic implications of this correspondence for the eigenfunctions of the Wheeler-DeWitt equation have been explored in [77, 78], which in particular allow for the derivation of a dual 'primon' [79] partition function for each wavefunction.

5. Discussion

The near-singularity limit offers a dramatic simplification of the equations of motion for metric components (and possible matter fields). The dynamics becomes ultralocal and fields at distinct spatial points follow independent trajectories in configuration space. In the Iwasawa frame, off-diagonal degrees of freedom freeze asymptotically while the evolution of the diagonal scale factors is dictated by a handful of simple reflection rules. This dynamics can naturally be reformulated in terms of billiards with hyperbolic domains. For most physically relevant theories, the billiard has finite volume and the dynamics features never-ending chaotic oscillations.

It may be interesting to revisit the chaos that arises from this oscillatory dynamics, especially in light of the last decade of research on the connection between black holes and chaos. Black holes are conjectured to be the best scramblers of information in nature [80]. This is a testament to their efficient way of processing information that falls through the horizon. An interesting way to diagnose scrambling is through an out-of-time ordered correlator (OTOC) in the framework of AdS/CFT. The holographic computation of this boundary four-point function involves a two-to-two scattering process near the horizon of the AdS black hole [81]. The OTOC is a semi-classical probe for the sensitivity to initial conditions [55]. In chaotic systems, it is expected to display an early-time period of exponential growth, with a characteristic quantum Lyapunov exponent, in analogy to (4.1). In quantum systems, the Lyapunov exponent was shown to be upper-bounded [82] and black holes saturate this bound. This is one possible characterization of the efficient scrambling of black holes. Note, however, that OTOCs really compute standard probes of chaos in the dual boundary theory and especially take the geometry exterior to the black hole horizon as input in the dual computation. This appears to be a quite different perspective on chaos than the BKL near-singularity chaos. It would be interesting to understand whether these two characterizations of chaos in black holes are related at all.

In the literature, most diagnostics for chaos (such as OTOCs) have been computed in analytically tractable models of black holes, such as Schwarzschild-like solutions or lower dimensional versions. However, as mentioned at the end of section 2, the Schwarzschild solution is quite fine-tuned in the space of solutions with a singularity, with Kasner exponents taking values at a corner of the possible range. Upon perturbations, this geometry is generally expected to settle into a more generic solution. Using this perspective, there has been recent progress in constructing perturbed asymptotically Anti-de Sitter black hole backgrounds with interior geometries displaying more general Kasner scalings, and even mixmaster oscillations, by turning on relevant sources in the boundary theory [28, 83–93]. This naturally triggers questions regarding possible imprints of BKL chaos in the theories holographically dual to these black holes.

Finally, we stress that it is important to bear in mind that the billiard picture is only exactly valid in the BKL limit $t \to 0$. Away from that limit, the walls are smooth potentials and no longer infinite Heaviside functions. Ultimately, one expects the singularity to get resolved in a complete theory of

quantum gravity. The classical theory should break down well before $t = 0$, when the volume of the spacelike slices reach Planckian size. If one wants to rely on the algebraic structures that emerge in the near-singularity region to constrain or guide possible quantum theories of gravity, it is essential to understand what remains of these structures when moving away from the strict BKL limit.

Acknowledgments

I would like to thank the organizing committee of the Modave Summer School in Mathematical Physics for the invitation to give these lectures and putting together such a nice program. I am grateful to the audience for their curiosity and questions that guided these notes. Finally, I would like to thank Sean Hartnoll for bringing up the topic of BKL chaos, which triggered my interest and our subsequent collaboration on this subject. The author is supported by a Leverhulme Early Career Fellowship and receives partial support from STFC consolidated grant ST/T000694/1.

References

[1] E.M. Lifshitz and I.M. Khalatnikov, *Investigations in relativistic cosmology*, *Adv. Phys.* **12** (1963) 185.

[2] V.A. Belinskii and I.M. Khalatnikov, *On the nature of the singularities in the general solution of the gravitational equations*, *Sov. Phys. JETP* **29** (1969) 911.

[3] V.A. Belinskii and I.M. Khalatnikov, *General solution of the gravitational equations with a physical singularity*, *Sov. Phys. JETP* **30** (1969) 1174.

[4] V.A. Belinskii, I.M. Khalatnikov and E.M. Lifshitz, *Oscillatory approach to a singular point in the relativistic cosmology*, *Adv. Phys.* **19** (1970) 525.

[5] V.A. Belinskii, E.M. Lifshitz and I.M. Khalatnikov, *The oscillatory mode of approach to a singularity in homogeneous cosmological models with rotating axes*, *Sov. Phys. JETP* **33** (1971) 1061.

[6] V.A. Belinskii, E.M. Lifshitz and I.M. Khalatnikov, *Construction of a general cosmological solution of the Einstein equation with a time singularity*, *Sov. Phys. JETP* **35** (1972) 838.

[7] R. Penrose, *Gravitational collapse and space-time singularities*, *Phys. Rev. Lett.* **14** (1965) 57.

[8] V. Belinskii and M. Henneaux, *The Cosmological Singularity*, Cambridge University Press (11, 2017).

[9] T. Damour, M. Henneaux and H. Nicolai, *Cosmological billiards*, *Class. Quant. Grav.* **20** (2003) R145 [hep-th/0212256].

[10] E.B. Bogomolny, B. Georgeot, M.J. Giannoni and C. Schmit, *Arithmetical chaos*, *Phys. Rept.* **291** (1997) 219.

[11] P. Bueno, P.A. Cano, R.A. Hennigar and M.-D. Li, *Kasner eons in Lovelock black holes*, *Phys. Rev. D* **110** (2024) 124015 [2409.00648].

[12] E. Cáceres, Á.J. Murcia, A.K. Patra and J.F. Pedraza, *Kasner eons with matter: holographic excursions to the black hole singularity*, *JHEP* **12** (2024) 077 [2408.14535].

[13] E. Kasner, *Geometrical theorems on Einstein's cosmological equations*, *Am. J. Math.* **43** (1921) 217.

[14] C.W. Misner, *Mixmaster universe*, *Phys. Rev. Lett.* **22** (1969) 1071.

[15] L. Bianchi, *Sugli spazí a tre dimensioni che ammettono un gruppo continuo di movimenti: memoria*, Tipografia della R. Accademis dei Lincei (1897).

[16] D.M. Chitre, *Ph.d. thesis*, *University of Maryland* (1972) .

[17] M.P. Ryan Jr., *Qualitative cosmology: diagrammatic solutions for bianchi type ix universes with expansion, rotation, and shear. i. the symmetric case*, *Annals of Physics* **65** (1971) 506.

[18] M.P. Ryan Jr., *Qualitative cosmology: Diagrammatic solutions for bianchi type ix universes with expansion, rotation, and shear. ii. the general case*, *Annals of Physics* **68** (1971) 541.

[19] T. Damour and M. Henneaux, *Chaos in superstring cosmology*, *Phys. Rev. Lett.* **85** (2000) 920 [hep-th/0003139].

[20] T. Damour and M. Henneaux, *Oscillatory behavior in homogeneous string cosmology models*, *Phys. Lett. B* **488** (2000) 108 [hep-th/0006171].

[21] T. Damour and M. Henneaux, E_{10}, BE_{10} *and arithmetical chaos in superstring cosmology*, *Phys. Rev. Lett.* **86** (2001) 4749 [hep-th/0012172].

[22] T. Damour, M. Henneaux and H. Nicolai, E_{10} *and a 'small tension expansion' of M theory*, *Phys. Rev. Lett.* **89** (2002) 221601 [hep-th/0207267].

[23] B.S. DeWitt, *Quantum theory of gravity. I. The canonical theory*, *Phys. Rev.* **160** (1967) 1113.

[24] E. Poisson, *A relativist's toolkit: The mathematics of black-hole mechanics*, Cambridge University Press (12, 2009).

[25] C.W. Misner, K.S. Thorne and J.A. Wheeler, *Gravitation*, Freeman, San Francisco (1973).

[26] S. Carlip and W. Hu, *Covariant Canonical Quantization and the Problem of Time*, *Fundam. Theor. Phys.* **216** (2024) 127 [2312.10272].

[27] C.W. Misner, *The Mixmaster cosmological metrics*, in *NATO Advanced Research Workshop on Deterministic Chaos in General Relativity*, 5, 1994 [gr-qc/9405068].

[28] M. De Clerck, S.A. Hartnoll and J.E. Santos, *Mixmaster chaos in an AdS black hole interior*, *JHEP* **07** (2024) 202 [2312.11622].

[29] J.A. Wheeler, *Superspace and the nature of quantum geometrodynamics*, *Adv. Ser. Astrophys. Cosmol.* **3** (1987) 27.

[30] D.A. Hejhal, *On eigenfunctions of the laplacian for hecke triangle groups*, in *Emerging applications of number theory*, pp. 291–315, Springer (1999).

[31] A. Csordás, R. Graham and P. Szépfalusy, *Level statistics of a noncompact cosmological billiard*, *Phys. Rev. A* **44** (1991) 1491.

[32] D.A. Hejhal and S. Arno, *On Fourier coefficients of Maass waveforms for $PSL(2,\mathbb{Z})$*, *Math. Comp.* **61** (1993) 245.

[33] G. Steil, *Eigenvalues of the Laplacian and of the Hecke operators for $PSL(2,\mathbb{Z})$*, Tech. Rep. P00022028 (3, 1994).

[34] M. Henneaux, M. Pilati and C. Teitelboim, *Explicit solution for the zero signature (strong coupling) limit of the propagation amplitude in quantum gravity*, *Phys. Lett. B* **110** (1982) 123.

[35] M. Henneaux, *The final Kasner regime inside black holes with scalar or vector hair*, *JHEP* **03** (2022) 062 [2202.04155].

[36] J. Demaret, J.L. Hanquin, M. Henneaux, P. Spindel and A. Taormina, *The fate of the mixmaster behavior in vacuum inhomogeneous Kaluza-Klein Cosmological Models*, *Phys. Lett. B* **175** (1986) 129.

[37] J. Demaret, M. Henneaux and P. Spindel, *Nonoscillatory behavior in vacuum Kaluza-Klein cosmologies*, *Phys. Lett. B* **164** (1985) 27.

[38] C. Saçlioglu, *Dynkin diagrams for hyperbolic kac-moody algebras*, *Journal of Physics A: Mathematical and General* **22** (1989) 3753.

[39] M. Henneaux, D. Persson and P. Spindel, *Spacelike singularities and hidden symmetries of gravity*, *Living Rev. Rel.* **11** (2008) 1 [0710.1818].

[40] T. Damour, S. de Buyl, M. Henneaux and C. Schomblond, *Einstein billiards and overextensions of finite dimensional simple Lie algebras*, *JHEP* **08** (2002) 030 [hep-th/0206125].

[41] J.D. Barrow, *Chaotic behavior in general relativity*, *Phys. Rept.* **85** (1982) 1.

[42] D. Hobill, A. Burd and A.A. Coley, *Deterministic chaos in general relativity*, vol. 332, Springer New York, NY (1994).

[43] E. Ott, *Chaos in Dynamical Systems*, Cambridge University Press, 2 ed. (2002).

[44] D. Hobill, D. Bernstein, M. Welge and D. Simkins, *The mixmaster cosmology as a dynamical system*, *Classical and Quantum Gravity* **8** (1991) 1155.

[45] A. Burd, N. Buric and G. Ellis, *A numerical analysis of chaotic behaviour in bianchi ix models*, *General relativity and gravitation* **22** (1990) 349.

[46] E. Artin, *Proceedings of the 7th latin american symposium on relativity and gravitation*, in *In Relativity and Gravitation: classical and quantum*, pp. 189–197, World Scientific, 1991.

[47] B.K. Berger, *Comments on the computation of liapunov exponents for the mixmaster universe*, *General relativity and gravitation* **23** (1991) 1385.

[48] K. Ferraz and G. Francisco, *Mixmaster numerical behavior and generalizations*, *Physical Review D* **45** (1992) 1158.

[49] K. Ferraz, G. Francisco and G. Matsas, *Chaotic and nonchaotic behaviour in the mixmaster dynamics*, *Physics Letters A* **156** (1991) 407.

[50] D.F. Chernoff and J.D. Barrow, *Chaos in the mixmaster universe*, *Phys. Rev. Lett.* **50** (1983) 134.

[51] N.J. Cornish and J.J. Levin, *The mixmaster universe: A chaotic Farey tale*, *Phys. Rev. D* **55** (1997) 7489 [gr-qc/9612066].

[52] J. Hadamard, *Les surfaces à courbures opposées et leurs lignes géodésiques*, .

[53] E. Artin, *Ein mechanisches system mit quasiergodischen bahnen*, in *Abhandlungen aus dem Mathematischen Seminar der Universität Hamburg*, vol. 3, pp. 170–175, Springer, 1924.

[54] N.L. Balazs and A. Voros, *Chaos on the pseudosphere*, *Phys. Rept.* **143** (1986) 109.

[55] Y.N. Larkin, Anatoly I. and Ovchinnikov, *Quasiclassical method in the theory of superconductivity*, *Sov Phys JETP* **28** (1969) 1200.

[56] E.P. Wigner, *On the statistical distribution of the widths and spacings of nuclear resonance levels*, in *Mathematical Proceedings of the Cambridge Philosophical Society*, vol. 47, pp. 790–798, Cambridge University Press, 1951.

[57] E.P. Wigner, *On the distribution of the roots of certain symmetric matrices*, *Annals of Mathematics* **67** (1958) 325.

[58] O. Bohigas, M.J. Giannoni and C. Schmit, *Characterization of chaotic quantum spectra and universality of level fluctuation laws*, *Phys. Rev. Lett.* **52** (1984) 1.

[59] O. Bohigas and M.-J. Giannoni, *Chaotic motion and random matrix theories*, in *Mathematical and Computational Methods in Nuclear Physics: Proceedings of the Sixth Granada Workshop Held in Granada, Spain, October 3–8, 1983*, pp. 1–99, Springer, 2005.

[60] O. Bohigas, *Random matrix theories and chaotic dynamics*, 1991.

[61] A. Altland and M.R. Zirnbauer, *Nonstandard symmetry classes in mesoscopic normal-superconducting hybrid structures*, *Phys. Rev. B* **55** (1997) 1142 [cond-mat/9602137].

[62] M.C. Gutzwiller, *Periodic orbits and classical quantization conditions*, *J. Math. Phys.* **12** (1971) 343.

[63] M.V. Berry, *Semiclassical theory of spectral rigidity*, *Proceedings of the Royal Society of London. A. Mathematical and Physical Sciences* **400** (1985) 229.

[64] S. Müller, S. Heusler, A. Altland, P. Braun and F. Haake, *Periodic-orbit theory of universal level correlations in quantum chaos*, *New Journal of Physics* **11** (2009) 103025 [0906.1960].

[65] M.L. Mehta, *Random matrices*, vol. 142, Elsevier (2004).

[66] J.S. Cotler, G. Gur-Ari, M. Hanada, J. Polchinski, P. Saad, S.H. Shenker et al., *Black Holes and Random Matrices*, *JHEP* **05** (2017) 118 [1611.04650].

[67] J. Bolte, G. Steil and F. Steiner, *Arithmetical chaos and violation of universality in energy level statistics*, *Phys. Rev. Lett.* **69** (1992) 2188.

[68] E. Bogomolny, B. Georgeot, M.-J. Giannoni and C. Schmit, *Chaotic billiards generated by arithmetic groups*, *Physical review letters* **69** (1992) 1477.

[69] R. Aurich, F. Scheffler and F. Steiner, *On the subtleties of arithmetical quantum chaos*, *Phys. Rev. E* **51** (1995) 4173.

[70] M.D. Clerck, "Arithmetic quantum chaos." https://www.youtube.com/watch?v=_yfkxGy06KI, Sept., 2025.

[71] J. Bolte, *Some studies on arithmetical chaos in classical and quantum mechanics*, *Int. J. Mod. Phys. B* **7** (1993) 4451.

[72] A. Terras, *Harmonic analysis on symmetric spaces–euclidean space, the sphere, and the Poincaré upper half-plane*, Springer (2013).

[73] K. Takeuchi, *Arithmetic triangle groups*, *Journal of the Mathematical Society of Japan* **29** (1977) 91.

[74] A.J. Feingold, A. Kleinschmidt and H. Nicolai, *Hyperbolic Weyl groups and the four normed division algebras*, *J. Algebra* **322** (2009) 1295 [0805.3018].

[75] A. Kleinschmidt, H. Nicolai and J. Palmkvist, *Modular realizations of hyperbolic Weyl groups*, *Adv. Theor. Math. Phys.* **16** (2012) 97 [1010.2212].

[76] S. Viswanath, *Embeddings of hyperbolic kac–moody algebras into e_{10}*, *Letters in Mathematical Physics* **83** (2008) 139 [0801.2586].

[77] S.A. Hartnoll and M. Yang, *The conformal primon gas at the end of time*, *JHEP* **07** (2025) 281 [2502.02661].

[78] M. De Clerck, S.A. Hartnoll and M. Yang, *Wheeler-DeWitt wavefunctions for 5d BKL dynamics, automorphic L-functions and complex primon gases*, *JHEP* **11** (2025) 160 [2507.08788].

[79] B. Julia, *Statistical theory of numbers*, in *Number Theory and Physics: Proceedings of the Winter School, Les Houches, France, March 7–16, 1989*, pp. 276–293, Springer (1990).

[80] Y. Sekino and L. Susskind, *Fast scramblers*, *JHEP* **10** (2008) 065 [0808.2096].

[81] S.H. Shenker and D. Stanford, *Stringy effects in scrambling*, *JHEP* **05** (2015) 132 [1412.6087].

[82] J. Maldacena, S.H. Shenker and D. Stanford, *A bound on chaos*, *JHEP* **08** (2016) 106 [1503.01409].

[83] S.A. Hartnoll, G.T. Horowitz, J. Kruthoff and J.E. Santos, *Diving into a holographic superconductor*, *SciPost Phys.* **10** (2021) 009 [2008.12786].

[84] R.-G. Cai, L. Li and R.-Q. Yang, *No inner-horizon theorem for black holes with charged scalar hairs*, *JHEP* **03** (2021) 263 [2009.05520].

[85] W. Li and M. Van de Moortel, *Kasner bounces and fluctuating collapse inside hairy black holes with charged matter*, *Ann. PDE* **11** (2025) 3 [2302.00046].

[86] M. Van de Moortel, *Violent nonlinear collapse in the interior of charged hairy black holes*, *Arch. Ration. Mech. Anal.* **248** (2024) 89 [2109.10932].

[87] A. Frenkel, S.A. Hartnoll, J. Kruthoff and Z.D. Shi, *Holographic flows from CFT to the Kasner universe*, *JHEP* **08** (2020) 003 [2004.01192].

[88] L. Sword and D. Vegh, *What lies beyond the horizon of a holographic p-wave superconductor*, *JHEP* **12** (2022) 045 [2210.01046].

[89] L. Sword and D. Vegh, *Kasner geometries inside holographic superconductors*, *JHEP* **04** (2022) 135 [2112.14177].

[90] R.-G. Cai, C. Ge, L. Li and R.-Q. Yang, *Inside anisotropic black hole with vector hair*, *JHEP* **02** (2022) 139 [2112.04206].

[91] D. Areán, H.-S. Jeong, J.F. Pedraza and L.-C. Qu, *Kasner interiors from analytic hairy black holes*, *JHEP* **11** (2024) 138 [2407.18430].

[92] R.-G. Cai, M.-N. Duan, L. Li and F.-G. Yang, *Clarifying Kasner dynamics inside anisotropic black hole with vector hair*, *JHEP* **04** (2025) 179 [2408.06122].

[93] J. Carballo, A.K. Patra and J.F. Pedraza, *Diving inside holographic metals*, *JHEP* **05** (2025) 072 [2408.07748].